Cenozoic tectonic evolution of the Qaidam basin and its surrounding regions (Part 3): Structural geology, sedimentation, and regional tectonic reconstruction

An Yin[*]
Structural Geology Group, School of Earth Sciences and Resources, China University of Geosciences, Beijing 100083, China
Permanent Address: Department of Earth and Space Sciences and Institute of Geophysics and Planetary Physics, University of California, Los Angeles, California 90095-1567, USA

Yu-Qi Dang
Min Zhang
Qinghai Oilfield Company, Dunhuang, Gansu Province, People's Republic of China

Xuan-Hua Chen
Institute of Geomechanics, Chinese Academy of Geological Sciences, Beijing, People's Republic of China

Michael W. McRivette
Department of Earth and Space Sciences and Institute of Geophysics and Planetary Physics, University of California, Los Angeles, California 90095-1567, USA

ABSTRACT

The Qaidam basin is the largest topographic depression inside the Tibetan plateau. Because of its central position, understanding the tectonic origin of the Qaidam basin has important implications for unraveling the formation mechanism and growth history of the Tibetan plateau. In order to achieve this goal, we analyzed regional seismic-reflection profiles across the basin and a series of thickness-distribution patterns of Cenozoic strata at different time slices. The first-order structure of the basin is a broad Cenozoic synclinorium, which has an amplitude ranging from >16 km in the west to <4 km in the east. The synclinorium has expanded progressively eastward across the Qaidam region: from the western basin against the Altyn Tagh fault at 65–50 Ma to the eastern basin at 24 Ma. The half-wavelength of the regional fold complex changes from ~170 km in the west to ~50 km in the east. The formation of the synclinorium was induced by an older thrust system initiated ca. 65–50 Ma in the northern margin and a younger thrust system initiated ca. 29–24 Ma in the southern basin margin. Cenozoic upper-crustal shortening decreases eastward across basin from >48% in the west to <1% in the east; the associated strain rates vary from 3.2×10^{-15} s^{-1} to 1.3×10^{-17} s^{-1}. The eastward decrease in upper-crustal shortening requires a progressive shift in crustal-thickening mechanisms across Qaidam basin, from dominantly upper-crustal shortening in the west to dominantly lower-crustal shortening in the east. Although sedimentation began synchronously at 65–50 Ma across the entire basin, the initiation ages of the southern and northern basin-bounding structures are significantly different; deformation started at 65–50 Ma in the north and at 29–24 Ma in the south. This information and the existing inference that the uplift of the Eastern Kunlun Range south of Qaidam basin began after 30–20 Ma imply that the Paleogene (65–24 Ma) Qaidam and Hoh Xil basins on both sides of the Eastern Kunlun Range may have been parts of a single topographic depression, >500 km wide in the north-south direction between the Qilian Shan and Fenghuo Shan thrust belts in the north and south. The development of this large Paleogene basin in central Tibet and its subsequent destruction and partitioning by the Neogene uplift of the Eastern Kunlun Range requires a highly irregular sequence of deformation, possibly controlled by preexisting weakness in the Tibetan lithosphere.

Keywords: Qaidam basin, Tibetan plateau, Eastern Kunlun Range, tectonics, deformation, upper crust, Cenozoic.

INTRODUCTION

With an average elevation of ~2800 m, the Cenozoic Qaidam basin is the largest topographic depression inside the 5000-m-high Tibetan plateau (Figs. 1 and 2). Despite its central position in Tibet, the tectonic origin of the basin has been debated. Bally et al. (1986) suggested that the basin formed over a large Cenozoic synclinorium. Burchfiel et al. (1989) postulated a basement-involved thrust belt across the basin. Métivier et al. (1998) proposed that the Qaidam basin developed via stepwise jumping of the northern Tibetan plateau margin in the Miocene (i.e., the bathtub-filling model; also see Meyer et al., 1998; Tapponnier et al., 2001; Sobel et al., 2003). Yin et al. (2002) inferred that the Qaidam basin has become an internally drained basin since the Oligocene; the trapping of Qaidam sediments was accomplished by progressive southward translation of the Altyn Tagh Range along the Altyn Tagh fault and the development of the Eastern Kunlun and Qilian Shan thrust belts (i.e., the sliding-door model). Wang et al. (2006) speculated that the Qaidam basin was extruded eastward from the Pamirs in western Tibet to its present position, during which a longitudinal river was developed along the basin axis between ca. 31 and 2 Ma.

The above tectonic models make specific predictions regarding the deformation history of the Qaidam basin and its relationship
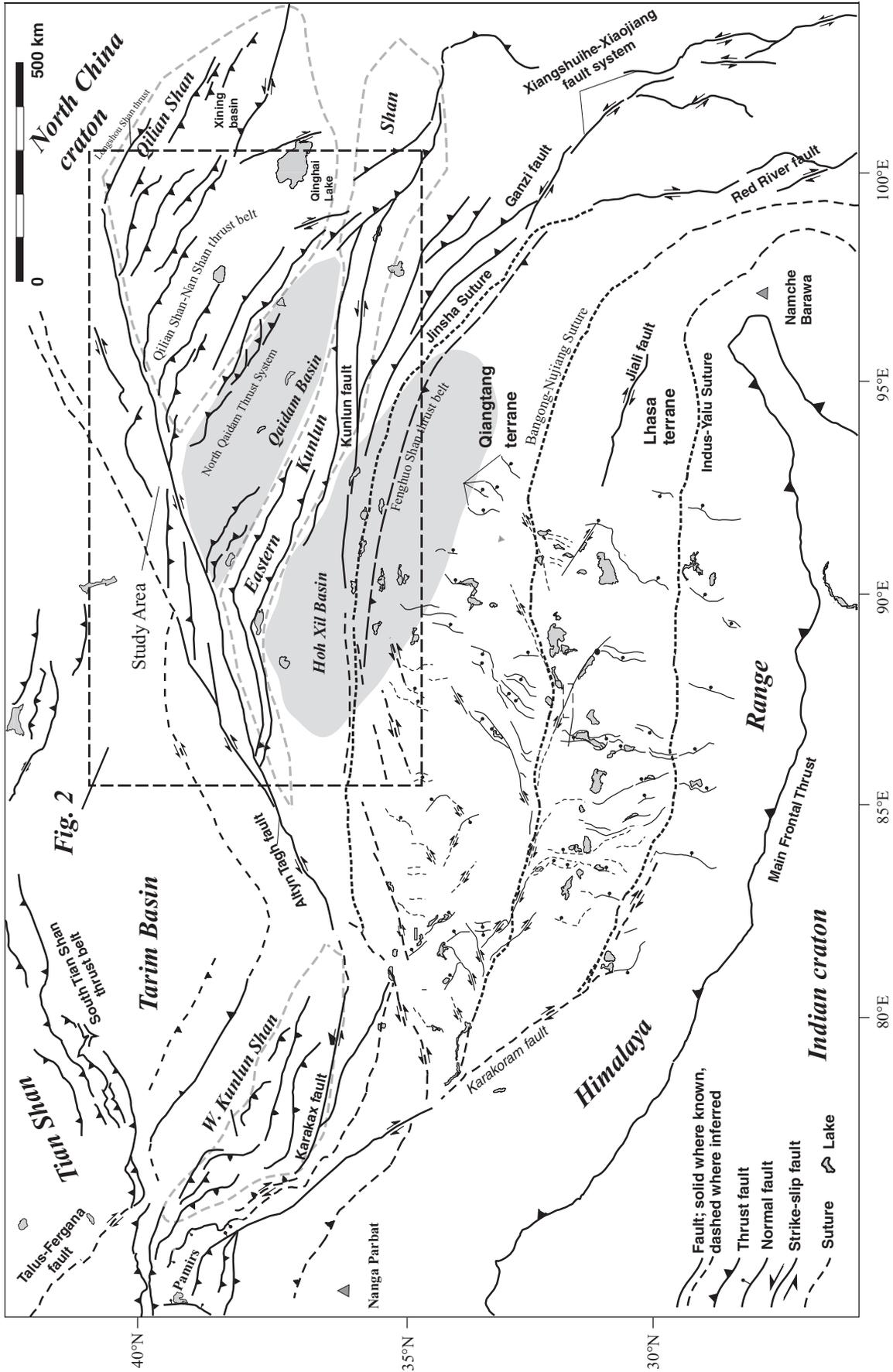
[*]Email: yin@ess.ucla.edu

Figure 1. Cenozoic tectonic map of the Tibetan plateau, modified from Taylor et al. (2003).

to basin-bounding structures. For example, the models of Métivier et al. (1998) and Wang et al. (2006) treat the Qaidam basin as a rigid block, while the models of Bally et al. (1986) and Burchfiel et al. (1989) require the Qaidam basin to be highly deformable. With regard to the basin-bounding structures, the stepwise-jump model of Métivier et al. (1998) predicts the southern basin-bounding thrust belt to have initiated before the northern basin-bounding thrust belt. In contrast, the extrusion model of Wang et al. (2006) requires the basin-bounding faults to have initiated synchronously and that the central Qaidam basin contains an eastward propagating sequence of alluvial and fluvial deposits between 33 and 3 Ma.

To evaluate the above models, we systematically analyzed seismic-reflection profiles and thickness-distribution patterns of Cenozoic strata across the Qaidam basin. The work presented here complements our three other companion studies surrounding the Qaidam basin, dealing with the Cenozoic southern Qilian Shan–Nan Shan thrust belt and early Paleozoic North Qaidam ultrahigh pressure metamorphic belt to the north (Yin et al., 2008a, 2007b) and the Cenozoic Qimen Tagh thrust belt to the south (Yin et al., 2007a). The studies in Yin et al. (2008, 2007a) emphasize the interaction between basin development and the evolution of its bounding thrust systems. In contrast, the study presented in this paper discusses the structural evolution of the basin. We first outline the geologic framework of the Qaidam basin. We then present our structural and sedimentological observations across the basin, and discuss the implications of our new observations for the Cenozoic tectonic reconstruction of the Qaidam basin and its relationship to the overall development of the Tibetan plateau. The Qaidam basin as discussed in this study is defined by its present morphological expression. Its boundaries in the Cenozoic may have changed through time, as implied in our study. All the shortening strain and the strain history obtained by this study are geographically specific for the present-day basin.

GEOLOGY OF THE QAIDAM BASIN

The Qaidam basin has a triangular geometry in map view, with an ~650 km northern margin, an ~700 km southern margin, and an ~300 km western margin (Fig. 1). Morphologically, the basin is bounded by the Qilian Shan, Altyn Tagh Range, and the Eastern Kunlun Range to the north, west, and south, respectively. Tectonically, the basin is bounded by the Qilian Shan–Nan Shan thrust belt (Burchfiel et al., 1989; Tapponnier et al., 1990) in the north, the left-slip Altyn Tagh fault in the west (e.g., Meyer et

al., 1998; Yin et al., 2002; Cowgill et al., 2000, 2003, 2004a, 2004b; Cowgill, 2007), and the Eastern Kunlun thrust belt in the south (Jolivet et al., 2003; Yin et al., 2007a) (Figs. 1 and 2). The basement of the Qaidam basin is composed of Precambrian–Silurian metamorphic rocks, which were overlain by Devonian–Cenozoic sedimentary strata (Huang et al., 1996). The metamorphic rocks are exposed along the rims of the basin, including the early Paleozoic North Qaidam ultrahigh pressure metamorphic gneiss (e.g., Yang et al., 2001; Song et al., 2005; Zhang et al., 2005; Yin et al., 2007b).

Despite a relatively high geothermal gradient in the uppermost part of the Qaidam basin, with values ranging from 31 to 70 mW/m, and a general decrease in heat flow from west to east (Nansheng, 2003), the mechanical strength of Qaidam lithosphere appears to be exceptionally strong, with an effective elastic thickness (Te) of ~70 km (Braitenberg et al., 2003). This Te value is significantly greater than that of 10–30 km for the rest of the Tibetan plateau (Braitenberg et al., 2003). The unusual strength of the Qaidam basin may be attributed to a significantly different lithospheric composition or the lack of fluid in the lower crust. For example, the basement of Qaidam crust may be oceanic in composition (Hsü, 1988; Gehrels et al., 2003a, 2003b), or the lower crust may be fluid poor (Jackson et al., 2004), making it exceptionally strong. Despite the unusually high strength, Qaidam crust is the thinnest in Tibet at ~45 km, as determined by several seismic studies (Zhu and Helmberger, 1998; Zhao et al., 2006; S.L. Li et al., 2006; Y.H. Li et al., 2006). The apparently high heat flow across the Qaidam basin could have been induced by hydrothermal circulation driven by the high topographic relief between the basin and its surrounding high mountain ranges (e.g., Person et al., 1996).

Cenozoic deformation of the Qaidam basin has been investigated in the past five decades since the initial work of Sun and Sun (1959) (also see a review on the history of geologic research in the Qaidam basin by Huang et al., 1996). Paleomagnetic studies across the basin indicate no rotation along its northern margin and ~16°–20° clockwise rotation in the southwestern basin in the Cenozoic (Dupont-Nivet et al., 2002; Chen et al., 2002; Halim et al., 2003; Sun et al., 2006). The variable rotation across the basin has been attributed to heterogeneous Cenozoic deformation (Yin et al., 2008). Initiation of deformation across the basin appears to be diachronous. Bally et al. (1986) showed that the Altyn Tagh fault and the structures along the western edge of the Qaidam basin were active since the middle Eocene. In contrast, Song and Wang (1993) inferred Neogene

initiation of thrusting in the southwestern the Qaidam basin.

The Qaidam basin preserves a complete record of Cenozoic sedimentation and has been the focus of numerous sedimentological and stratigraphic studies (Bally et al., 1986; Wang and Coward, 1990; Song and Wang, 1993; Huang et al., 1996; Zhang, 1997; Métivier et al., 1998; Xia et al., 2001; Yin et al., 2002; Sobel et al., 2003; Sun et al., 2005; Rieser et al., 2005, 2006a, 2006b; Zhou et al., 2006). For example, Cenozoic basin history has been established by analyzing thickness distribution (Huang et al., 1996), paleocurrent analysis (Hanson, 1998), lithofacies patterns (e.g., Zhang, 1997), sandstone petrology (Rieser et al., 2005), and $^{40}Ar/^{39}Ar$ detrital-mica ages (Rieser et al., 2006a, 2006b). In addition, Cenozoic chronostratigraphy of the basin has been investigated in detail by using fossils (i.e., spores, ostracods, and pollen), basin-wide seismic stratigraphic correlation, magnetostratigraphic studies, and fission-track dating of detrital grains (Huo, 1990; Qinghai Bureau of Geology and Mineral Resources, 1991; Yang et al., 1992, 1997, 2000; Song and Wang, 1993; Huang et al., 1996; Xia et al., 2001; Nansheng, 2002; Sun et al., 1999, 2005). These studies suggest that Cenozoic sedimentation in the Qaidam basin expanded eastward from the Paleocene and early Eocene in the west and Miocene–Pliocene in the east, with its main depositional center consistently located along the central axis of the basin.

Early structural studies of the Qaidam basin based on interpretation of seismic profiles did not consider the role of thrust-related folding and the complexity of thrust-system geometry. This has led to relatively small amounts of total estimated shortening across the basin (i.e., ~10 km; Huang et al., 1996; Dang et al., 2003; Zhou et al., 2006). There has also been a lack of effort in evaluating relationships between syntectonic growth strata and Cenozoic contractional structures that has hindered our understanding of the temporal development of the basin.

In this paper we present seven regional geologic cross sections and eight Cenozoic isopach maps (Fig. 3). Using these data, we show that Cenozoic sedimentation occurred synchronously across the basin since the Paleocene–early Eocene (65–50 Ma). However, initiation of deformation across the basin is diachronous, starting first in the northwest at 65–50 Ma and subsequently propagating to the southern and eastern margins of the basin at 29–24 Ma.

STRUCTURAL GEOLOGY

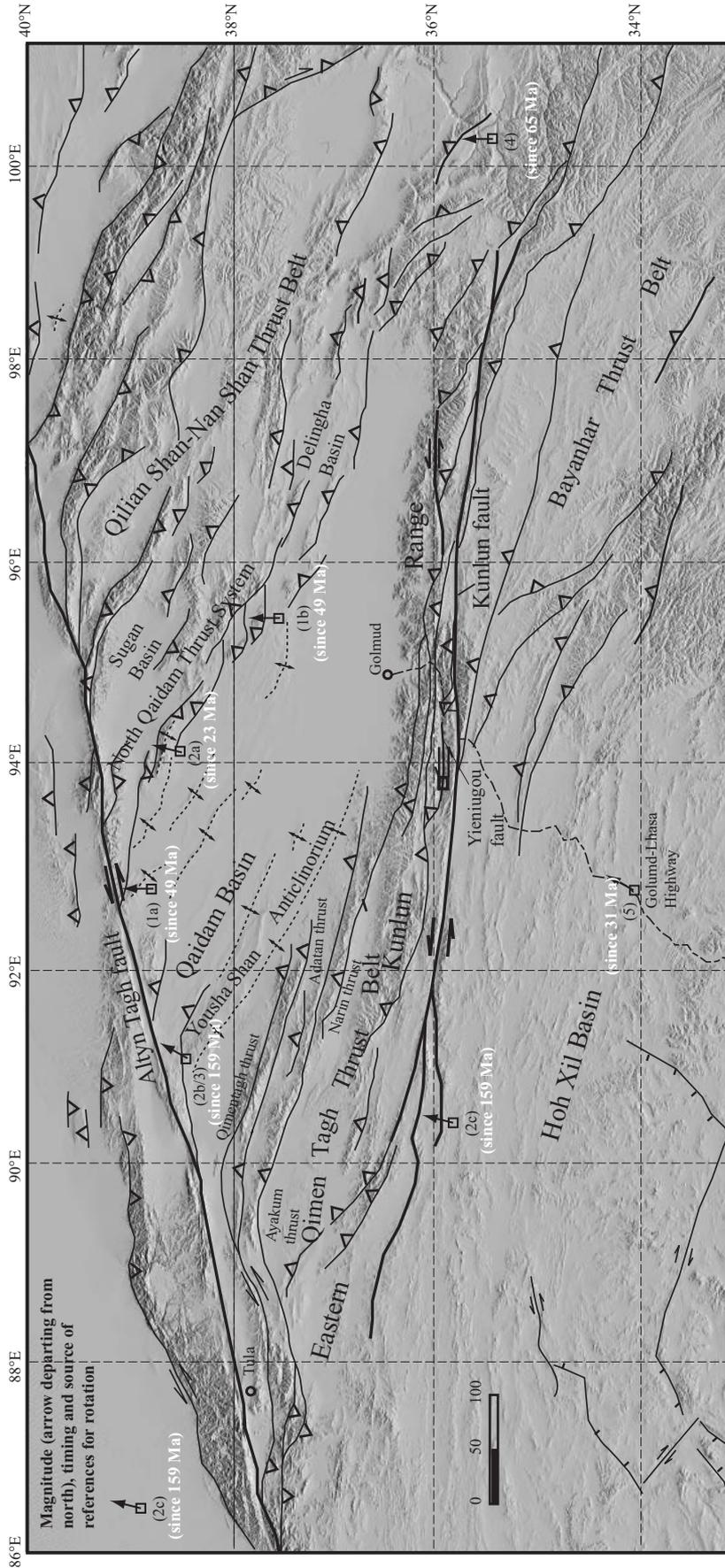In order to construct true-scale geologic cross sections, we first interpreted seismic-reflection

Figure 2. Cenozoic tectonic map of northern and central Tibet, after Yin et al. (2007a, 2007b). The magnitude and timing of rotation relative to Eurasian reference pole across Qaidam and Hoh Xil basins are also shown. Data points: 1a—no clockwise rotation recorded in the middle Eocene–early Oligocene strata (49–28.5 Ma) (from Dupont-Nivet et al., 2002); 1b—no clockwise rotation recorded in the middle Eocene–early Oligocene strata (49–28.5 Ma) (from Dupont-Nivet, 2002); 2a—~14° clockwise rotation since the end of the Paleogene (ca. 23 Ma) (from Chen et al., 2002); 2b/3—to ~29° clockwise rotation since the Late Jurassic (from Chen et al., 2002; Halim et al., 2003); 2c—~15° clockwise rotation since the late Oligocene (28.5–23 Ma) (from Chen et al., 2002); 4—no rotation throughout the Cenozoic (from Sun et al., 2006); 5—~29° clockwise rotation since ca. 31 Ma.
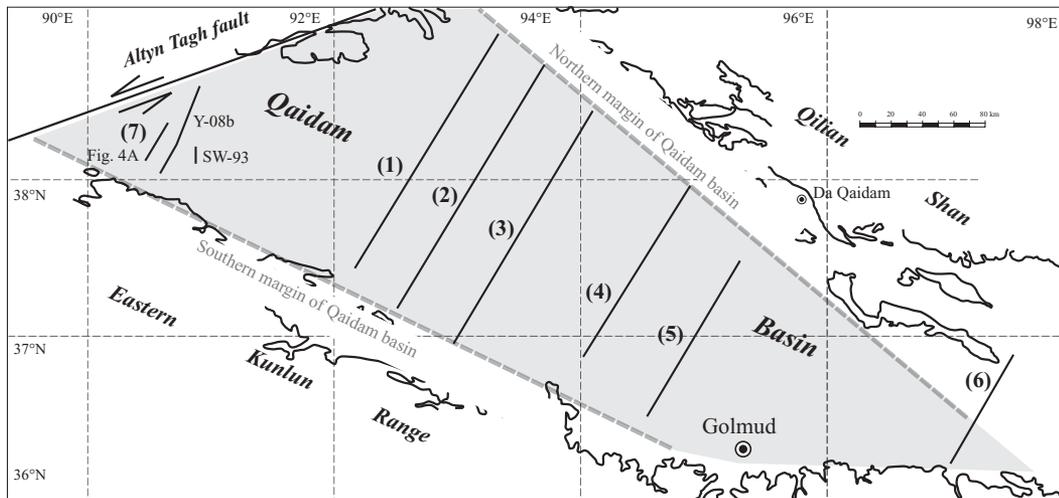
Figure 3. Locations of seven seismic lines discussed in the text. Also shown are three seismic lines in Figure 4. Thick dashed lines show the present-day northern and southern margins of the Qaidam basin. SW-93—location of seismic line from Song and Wang (1993); Y-08b—location of geologic cross section from Yin et al. (2007a).

profiles in the time domains and then converted them to the depth domains using known velocity values. The zero depth in all sections corresponds to a reference elevation of 2750 m. In general, the top 16–18 km of the interpreted sections were constructed based on seismic profiles (i.e., two-way traveltime equal to ~6 s), whereas sections below 16–18 km are drawn by downward projection of the structures imaged in the seismic profiles. The locations of the interpreted seismic sections are shown in Figure 3 and examples of the seismic profiles analyzed in this study and their interpretations are shown in Figure 4. The age assignments of Cenozoic stratigraphic units and regionally correlative seismic reflectors are shown in Table 1 (Yin et al., 2008, 2007a).

Interpreted Seismic Section 1

Structural Geology

The overall architecture of section 1 is a large-scale synclinorium that spans more than 170 km in the northeast-southwest direction (i.e., the half-wavelength of the fold) and has >16 km amplitude (Fig. 5). The fold is expressed by broadly folded Pliocene and Quaternary strata in the top, with complex contractional structures in the Paleocene–Miocene strata below the fold limbs: in the south is a south-directed fault-bend-fold system and in the north is a passive-roof thrust duplex, part of the North Qaidam triangle zone (Fig. 5). The duplex system repeats Jurassic and Paleogene strata (Jr to E3–2) with its leading-edge thrust exposed in the North Qaidam thrust system (Yin et al., 2008). The Yousha Shan backthrust is a blind fault, terminating at a north-verging fault-propagation fold (Fig. 5); its maximum slip is ~2.5 km. Though counterintuitive, south-directed thrusts dominate the Qimen

Tagh Range, which bounds the Qaidam basin to the southwest (Yin et al., 2007a).

Tilting of the northern synclinorium limb can be explained easily by the development of a triangle zone in the northern basin. However, explaining the northward tilting of the southern synclinorium limb is more difficult. One possibility is that tilting was produced by motion on a north-dipping thrust ramp in the southern section. The tilting could alternatively be caused by thrusting on a deep-seated south-dipping fault (i.e., the inferred deep-seated Eastern Kunlun thrust in Fig. 5).

When considering cross-section balancing, the observed Cenozoic folds and thrusts may be explained by the presence of a basal thrust in the pre-Jurassic basement, which we refer to as the Main Qaidam detachment (Fig. 5). This fault consists of three ramps connected by two flats at depths of 12 and 28 km, respectively. Our proposed mid-crustal Main Qaidam detachment is broadly compatible with the similar concept proposed by Burchfiel et al. (1989) for the style of contractional deformation across the Qaidam basin. The difference between our fault and that postulated by Burchfiel et al. (1989) is that our detachment has a considerable variation of geometry in the basement from a simple sub-horizontal décollement.

It is also possible that the basement-involved thrusts in the Qaidam basin sole into the lower crust where the crustal strength is weakest, if it follows wet quartz rheology (Chen and Molnar, 1983). Alternatively, the Qaidam crust could have a mafic composition or the lower crust may lack fluid activity, making it strong enough to localize shear deformation (Jackson et al., 2004).

Growth-Strata Relationships and Timing of Deformation

Unit E1+2 was deposited across the entire Qaidam basin and exhibits growth-strata relationships above the northern triangle zone (Fig. 5), suggesting the onset of deformation at 65–50 Ma in the northern section. The age of south-directed thrusting in the southern Qaidam basin is much younger, starting ca. 29 Ma, as indicated by growth strata of unit N1 associated with development of the south-verging fault-bend fold (Fig. 5).

Cenozoic Strain and Strain Rate

Line balancing of unit E1+2 yields 84 km shortening (lower diagram of Fig. 5) and a shortening strain of 32.3%. The strain was accommodated over 65–50 m.y., which yields an average strain rate of $1.5–2.0 \times 10^{-16}$ s^{-1}.

TABLE 1. MESOZOIC AND CENOZOIC STRATIGRAPHY OF QAIDAM BASIN

| Unit names	Symbol	Geologic time	Age
Dabuxun Yanqiao Formation	Q2	Holocene	0.01 Ma–present
Qigequan Formation	Q1	Pleistocene	1.8–0.01 Ma
Shizigou Formation	N2-3	Pliocene	5.3–1.8 Ma
Shangyoushashan Formation	N2-2	late Miocene	11.2–5.3 Ma
Xiayoushashan Formation	N2-1	early and middle Miocene	23.8–11.2 Ma
Shangganchaigou Fm	N1	late Oligocene	28.5–23.8 Ma
Upper Xiaganchaigou Fm	E3-2	early Oligocene	37–28.5 Ma
Lower Xiaganchaigou Fm	E3-1	middle Eocene–late Eocene	49–37 Ma
Lulehe Fm	E1+2	Paleocene–Early Eocene	>54.8–49 Ma
(Jurassic strata, locally overlain by Cretaceous beds)	Jr	Jurassic-Cretaceous	206–65 Ma
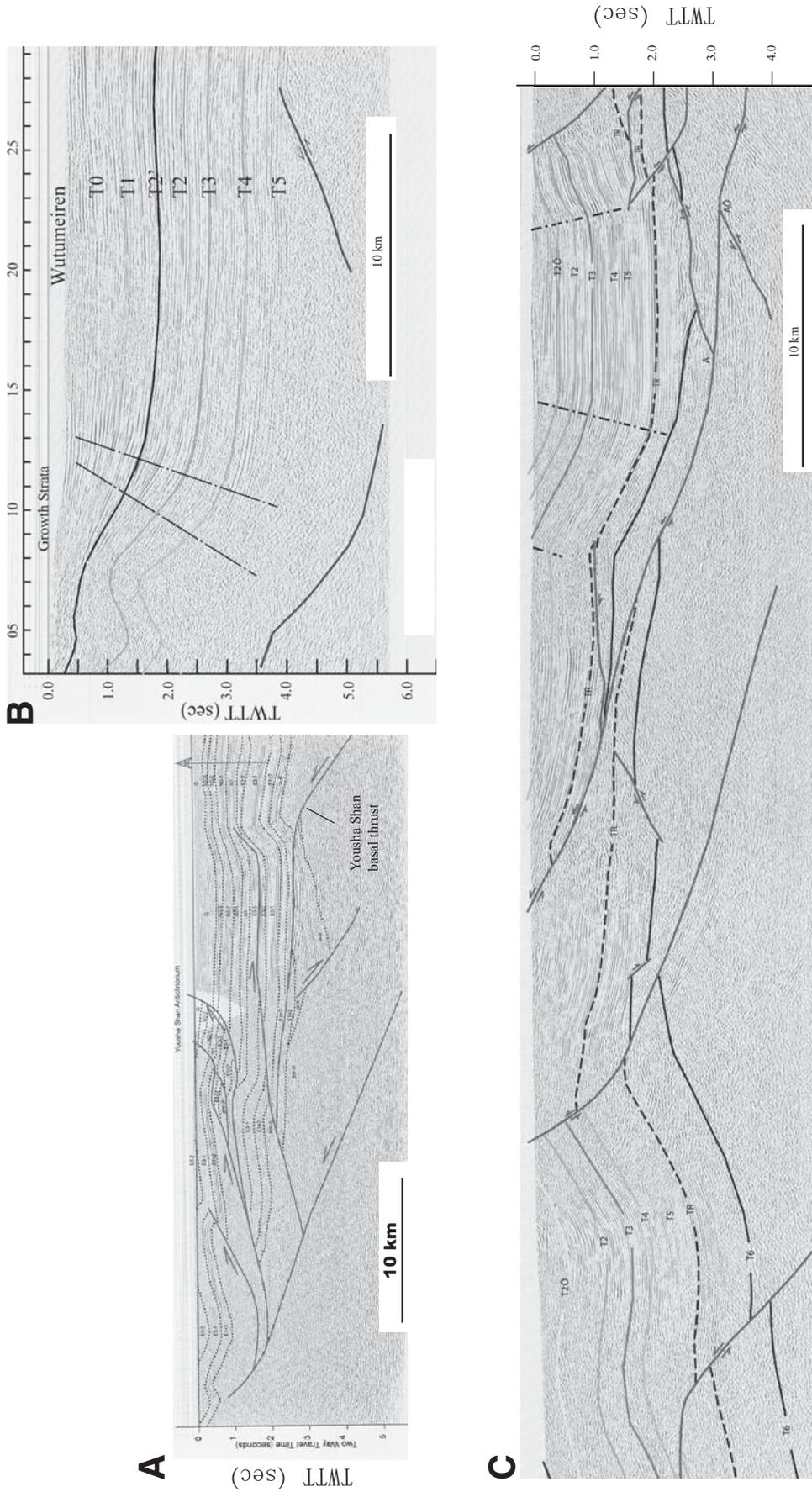
Figure 4. Examples of seismic lines used in this study. (A) Section 7. (B) Southernmost segment of section 3. (C) Northernmost segment of section 4. See Figure 3 for locations. T0 to T6 are regionally correlative seismic reflectors; their relationships to Mesozoic and Cenozoic stratigraphic units are shown in Table 1. TWTT—two-way traveltime. T0 to T6 are regionally correlative reflectors. T0 at the top of the Shizigou formation, T1 at the top of the Shangyoushashan formation, T2 at the top of the Xiayoushashan formation, T3 at the top of the Shangganchaigou formation, T4 at the top of the Upper Xiaganchaigou formation, T5 at the top of the Lower Xiaganchaigou formation, TR at the top of the Lulehe formation, and T6 at the top of the Jurassic-Cretaceous strata.
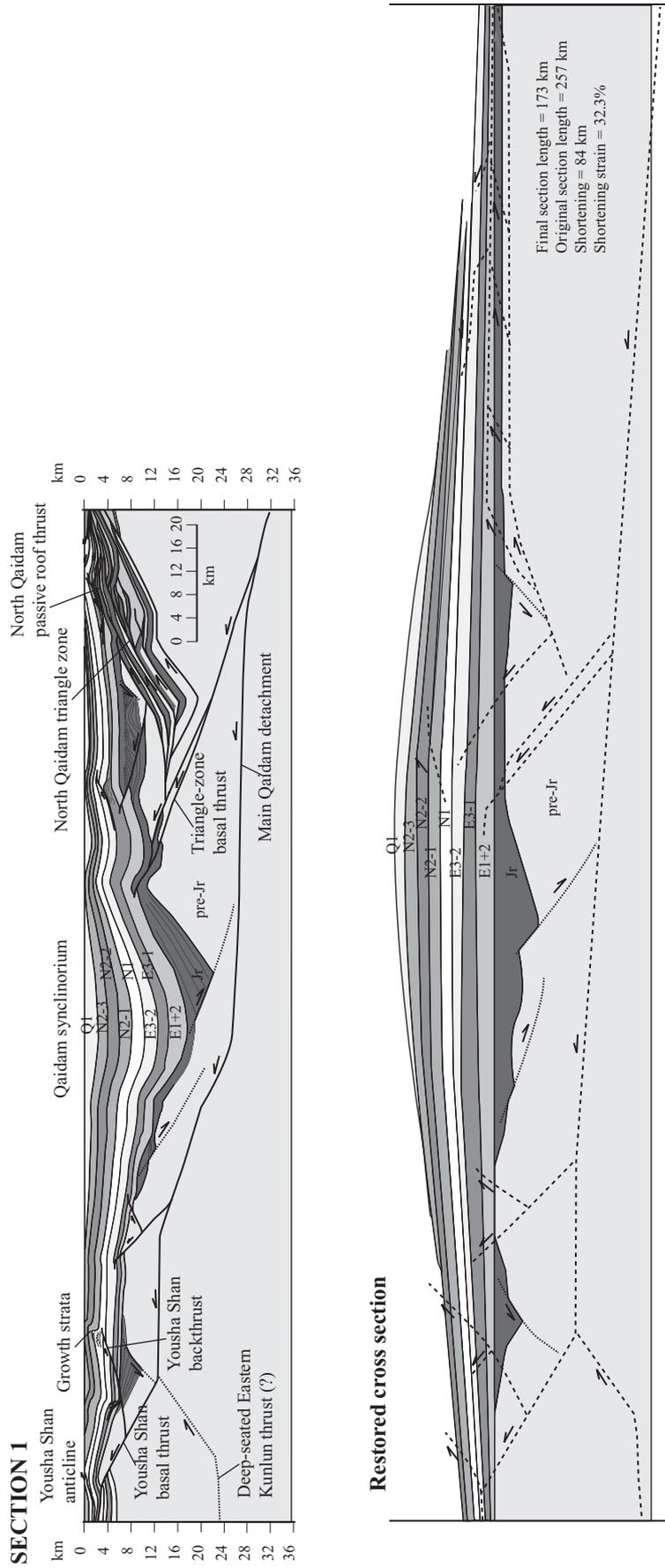
Figure 5. Geologic cross section of line 1 (upper diagram) and the restored section (lower diagram). See Figure 3 for location. The total amount of shortening is 84 km, with a shortening strain of 32.3%. Jr—Jurassic. See Table 1 for definition of lithologic units.
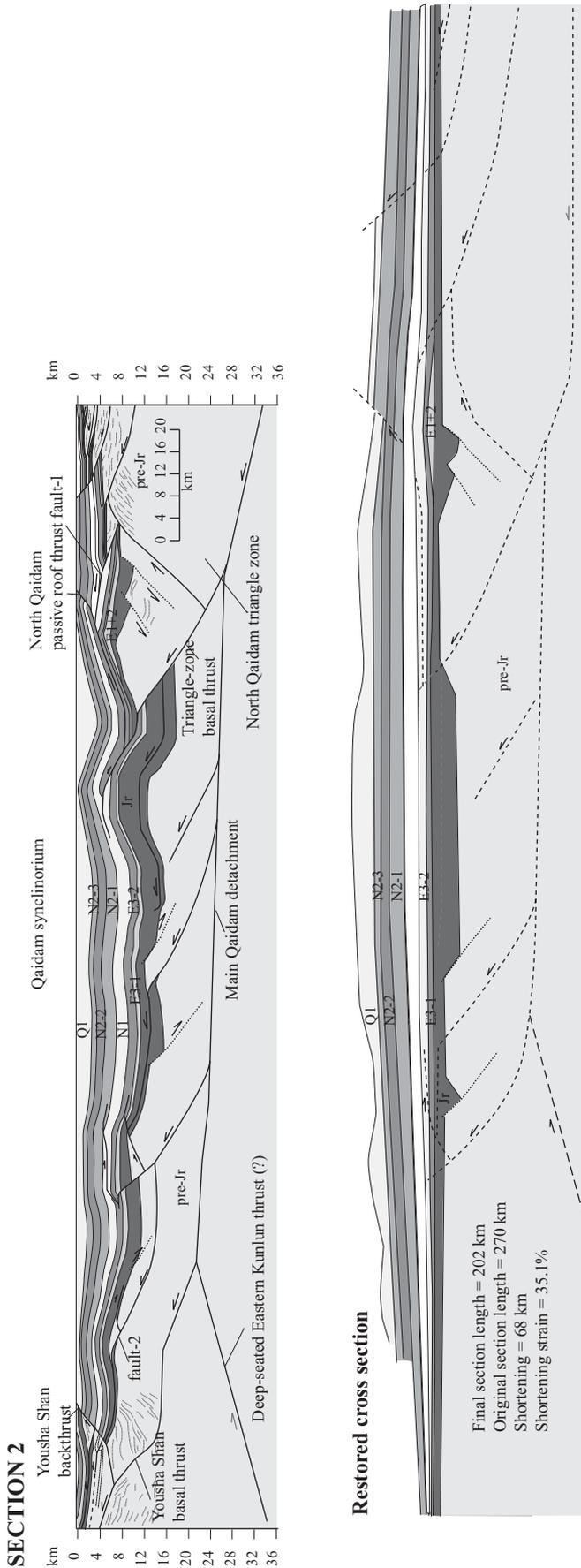
Figure 6. Geologic cross section of line 2 (upper diagram) and the restored section (lower diagram). See Figure 3 for location. The total amount of shortening is 68 km, with a shortening strain of 35%. Jr—Jurassic. See Table 1 for definition of lithologic units.

Mesozoic Deformation

Jurassic sedimentary strata are highly discontinuous with variable thickness along section 1. The sediments exhibit growth-strata geometry in half-grabens bounded by extensional faults with normal separation varying from 2 to 9 km. Because there are no matching cutoffs in the footwall basement rocks below the extensional structures, the above estimates are likely minimum values.

Interpreted Seismic Section 2

Structural Geology

This section, located 40 km east of section 1, exhibits a large synclinorium that has a smaller amplitude (~12 km) and broader fold geometry than that in section 1. In addition, the North Qaidam triangle zone changes from having dominantly north-directed thrusts in section 1 to dominantly south-directed thrusts in section 2.

Slip on the Yousha Shan backthrust is ~7 km, which is significantly greater than ~2 km in section 1; the fault cuts the whole Cenozoic section rather than casting as a blind structure as in section 1 (Fig. 6; cf. Fig. 5). The backthrust could root below the Eastern Kunlun Range to the south, but continuous reflectors across its downward projection preclude this possibility (Fig. 6).

Cenozoic strata are subhorizontal in the central part of the section and dip gently northward in the south (Fig. 6). Similar to section 1, Cenozoic deformation in the upper crust can be explained by the basement-involved thrusts soling into a basal décollement that has two flats and three ramps (i.e., the Main Qaidam detachment; Fig. 6), similar to those in section 1. Although the main thrust flats in both sections lie at a depth of ~28 km, the main flat in section 2 is significantly longer and implies the trends of the connected thrust ramps in the Qaidam basement are oblique to the thrust transport direction. As in section 1, a deep-seated south-dipping thrust may be below the Eastern Kunlun Range and the southern Qaidam basin (i.e., the deep-seated Eastern Kunlun thrust; Fig. 6).

Growth-Strata Relationships and Timing of Deformation

Unit E1+2 is only present on top of an anticline in the northern part of section 2 (Fig. 6). This relationship alone suggests that deposition of unit E1+2 predates the anticline. The lateral pinch-out geometry of unit E1+2 could have resulted from early synclinal folding that was later inverted into an anticline. This interpretation suggests that the deformation in the northern part of the section started ca. 65–50 Ma during deposition of unit E1+2. Alternatively, the pinch-out geometry of unit E1+2 may have been

induced by post-E1+2 synclinal folding and subsequent erosion of its limbs. This interpretation would imply a younger initiation age of deformation in the northern part of the section.

The thickness of unit E3–1 exhibits minor variation in section 2, the central portion being slightly thicker than that in the southern and northern parts of the section. This relationship suggests that a broad syncline with amplitude <1 km was developed during deposition of unit E3–1. Because the thickness of E3–1 does not change across the hanging wall of the basal thrust of the North Qaidam triangle zone, the initiation of this structure must postdate deposition of unit E3–1 (i.e., postdating late Eocene; see Table 1).

Thickness variation is more pronounced for unit E3–2 in section 2, which thickens at the synclinorium core in the section and thins toward the fold limbs. This suggests that the synclinal folding was still active during deposition of unit E3–2 (early Oligocene; see Table 1). A prominent change in the thickness of unit E3–2 occurs in the hanging wall of the triangle-zone basal thrust in the northern part of the section (Fig. 6), indicating initiation of the triangle zone during its deposition. This timing of deformation is significantly younger than the initiation age of the triangle-zone structures in sections 1 and 3 at 65–50 Ma (see Figs. 5 and 7 and related discussion).

The passive-roof thrust of the triangle zone in the northern part of the section was initiated during deposition of unit N1 (late Oligocene; see Table 1). This is reflected by a prominent change in the unit thickness across the fault: thinner in its hanging wall and significantly thicker in its footwall (Fig. 6). The inferred Oligocene age is consistent with the growth-strata relationship across a minor north-dipping thrust (fault 1 in Fig. 6) that merges with the passive-roof fault; across the fault unit N1 is thicker in its footwall than in its hanging wall, suggesting motion on fault 1 and thus its kinematically linked passive-roof fault was coeval with deposition of unit N1.

There is no observable thickness change across the Yousha Shan backthrust for units E3–1 and E3–2 in the southern part of the section (Fig. 6). Because unit N1 is only partially exposed in the hanging wall of the Yousha Shan backthrust, it is not possible to compare thickness variation across the fault. However, the constant thickness of units E3–1 and E2–3 across the backthrust suggests its initiation postdates their deposition (i.e., the backthrust is younger than early Oligocene). The exact age of initiation for the Yousha Shan backthrust may be obtained from the age of fault 2, which merges with the backthrust. Thinning of unit N1 at the crest of a fault-bend fold anticline associated

with fault 2 indicates that motion on this fault started during deposition of unit N1 (29–24 Ma) and has remained active (Fig. 6).

Strain and Strain Rate

The total amount of shortening over the ~200 km section is 68 km, which yields a total shortening strain of 35%. Because most of this deformation occurred over a period of 29 m.y., it yields an average strain rate of 3.8×10^{-16} s^{-1}.

Mesozoic Structures

The overall Jurassic structure is a symmetric graben, with Jurassic strata being thickest inside the graben and thinnest outside the graben. The section shows no evidence for reactivation of the early extensional faults by later thrusts, as they generally dip in the opposite directions (Fig. 6).

Interpreted Seismic Section 3

Structural Geology

This section lies 46 km east of section 2 (Fig. 7). In sharp contrast to section 2, the dominant structures are north-directed thrusts rather than south-directed thrusts. The most prominent north-directed thrust is the North Qaidam passive-roof thrust, which cuts upward from the basement and flattens into unit E3–1; its maximum displacement is <2 km (Fig. 7). Other north-directed thrusts either die out into fault-propagation folds of the Suppe and Medwedeff (1990) type or fault-bend folds of the Suppe (1983) type.

Like sections 1 and 2, the first-order structure along section 3 is a large synclinorium. The fold amplitude is ~10 km, slightly less than that in section 2 (~12 km) and significantly less than that in section 1 (>16 km). The magnitude of slip on individual faults cutting across the base of the Cenozoic strata is <2 km, which is insufficient to explain the observed fold amplitude. Thus, either deep-seated thrusts or distributed contraction is required in the middle and lower crust in the southern Qaidam basin to create the observed structural relief. To be consistent with the structural style observed in sections 1 and 2, we hypothesize a north-dipping thrust ramp below the northern edge of the Qaidam basin in the middle crust, which is equivalent to the triangle-zone basal thrust seen in sections 1 and 2 (Fig. 7A; cf. Figs. 5 and 6). The rest of the north-directed thrusts could either sole into a south-directed basal thrust as in sections 1 and 2 (i.e., the Main Qaidam detachment) (Fig. 7A), or into a north-directed and south-dipping thrust extending below the Eastern Kunlun Range (i.e., the Eastern Kunlun thrust) (Fig. 7C; cf. Fig. 5). In the first interpretation (Fig. 7A), it is possible that the deep-seated south-dipping Eastern Kunlun thrust lies below the Main

Qaidam detachment; in this case the detachment transport direction is south directed. The second interpretation implies that the Qaidam lower crust has been subducted below the Eastern Kunlun Range and the Qilian Shan, predicting a top-north sense of shear on the detachment. In any case, both interpretations in Figures 7A and 7C require the presence of a subhorizontal detachment at a depth of ~28 km, but there is no need for a south-dipping basin-bounding thrust exposed at the surface along the southern Qaidam basin margin.

Growth-Strata Relationships and Timing of Deformation

Unit E1+2 is thickest over the Qaidam synclinorium axis and thins southward to the Eastern Kunlun Range and northward over a fault-bend fold above the North Qaidam passive-roof thrust (Fig. 7A). The unit pinches out before reaching to the southern end of the section. The above relationship suggests that the synclinorium and the triangle zone were both developed during deposition of unit E1+2. This timing of deformation is similar to that for the northern part of section 1 at 65–50 Ma, but older than that for the northern part of section 2 at 29–24 Ma. Like in sections (1) and (2), the initiation age of deformation in the southern part of section 3 is younger at 29–24 Ma. This is indicated by the growth-strata relationship between unit N1 and the underlying anticline above the Adatan thrust (Fig. 7).

Strain and Strain Rate

The total amount of shortening calculated by line balancing of unit E3–1 is 41 km across the 190-km-long cross section. This yields a total shortening strain of 17%. Because this strain was accomplished since 65–50 Ma, it leads to an estimated average strain rate between 0.8 and 1.0×10^{-16} s^{-1}.

Mesozoic Structures

Section 3 exhibits a horst structure in the center bounded by listric normal faults with Jurassic strata deposited above the horst and in the flanking half-grabens (Fig. 7). The magnitude of normal separation is ~3–4 km. The fanning geometry of growth strata above extensional faults can be recognized in the section (Fig. 7A).

Interpreted Seismic Section 4

Structural Geology

This section, located ~84 km east of section 3, exhibits a broad synclinorium with a much smaller amplitude (<5 km) than those in sections 1 (>16 km), 2 (~12 km), and 3 (~10 km) (Fig. 8). In the north, section 4 is dominated by a south-directed imbricate thrust system,
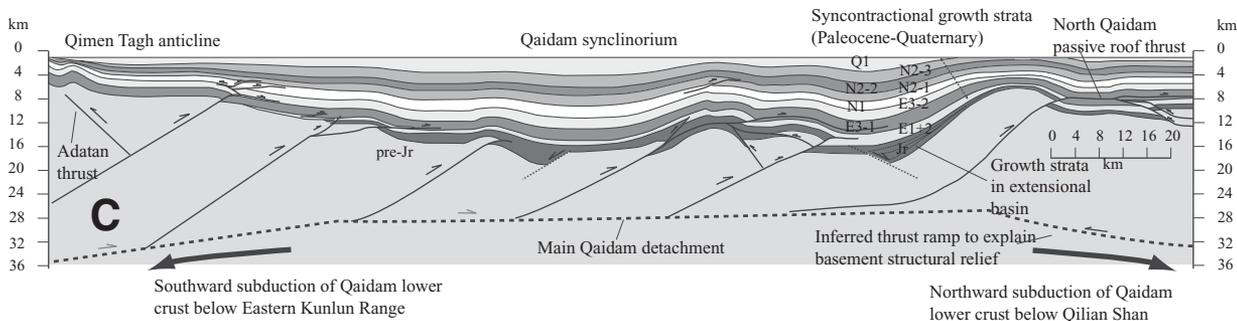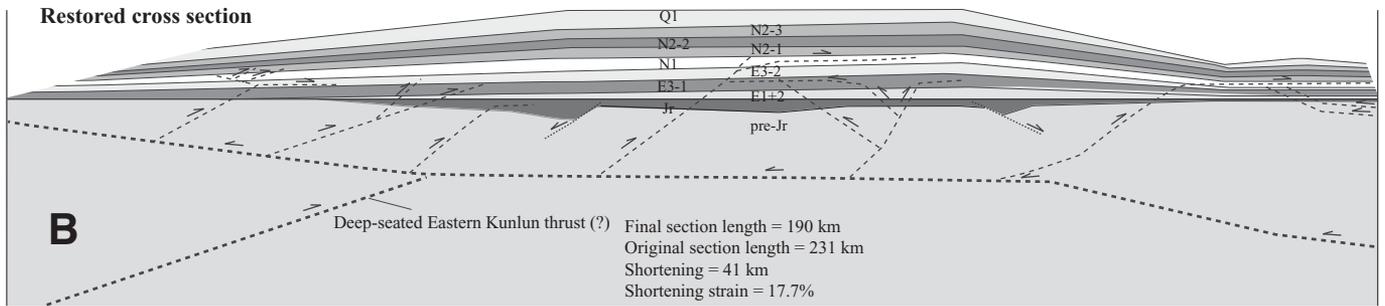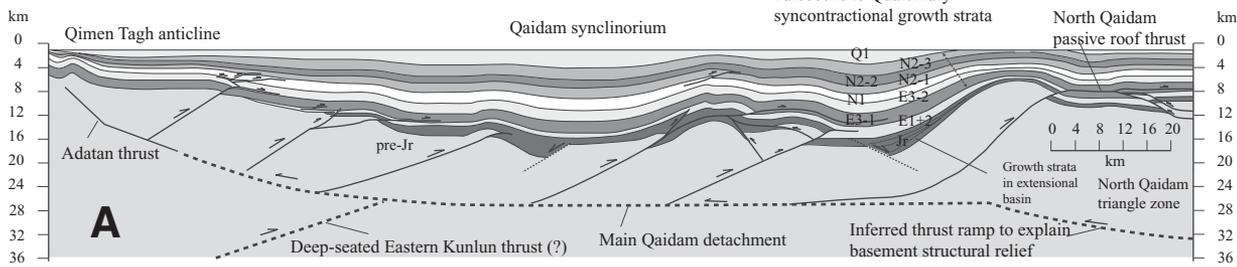
SECTION 3

Figure 7. Geologic cross section of line 3 (upper diagram) and the restored section (lower diagram). See Figure 3 for location. The total amount of shortening is 41 km, with a shortening strain of 17%. Jr—Jurassic. See Table 1 for definition of lithologic units.

whereas in the south across the Qaidam synclinorium axis Jurassic and Cenozoic strata are essentially undeformed. The north-dipping basin floor in the south can be explained by the presence of a gentle north-dipping thrust ramp in the middle crust that links with a subhorizontal detachment at a depth of ~24 km.

Growth-Strata Relationships and Timing of Deformation

There is no appreciable thickness variation for units E1+2 to N1, but unit N2–1 and younger strata thicken toward the axial region of the Qaidam synclinorium. This suggests folding started during deposition of unit N2–1 (24 Ma). This age of synclinal folding is significantly younger than the initiation age for the Qaidam synclinorium at 65–50 Ma in sections 1 and 3, suggesting that the synclinorium grew eastward and reached section 4 ca. 24 Ma.

Strain and Strain Rate

The total amount of shortening across the 167-km-long section 4 is 20 km, which yields a total shortening strain of 11%. Over 24 m.y., the average strain rate is 0.5–0.7×10^{-16} s^{-1}.

Mesozoic Structure

Jurassic strata are restricted to the central and northern parts of section 4 and are distributed discontinuously in small grabens (Fig. 8). Normal separation on extensional faults is between 1 and 4 km. The estimates are likely minimum values because some faults place Jurassic strata over pre-Jurassic basement.

Interpreted Seismic Section 5

Structural Geology

This section is 62 km east of section 4 (Fig. 9). The Qaidam synclinorium has ampli-

tude of 3–4 km in this section. Two south-directed thrusts are below the northern limb of the synclinorium: the southern fault (fault 2 in Fig. 9) produces a fault-propagation fold, and the northern fault (fault 1 in Fig. 9) forms the basal thrust of a small triangle zone. Except a minor south-dipping thrust with hundreds of meters of slip (fault 3), the southern section is undeformed. The basement of the southern Qaidam basin tilts northward at an angle of ~4°–5°, which cannot be explained by motion on fault 3 in Figure 9. Because of this, we infer the presence of a gently north dipping décollement at depths of ~15–22 km; a deep-seated south-dipping thrust may be below the southern Qaidam basin that merges upward with the thrust décollement (Fig. 9). A key difference between the geometry of the Main Qaidam detachment shown in this section and that in sections 1–4 is that the upper-crustal
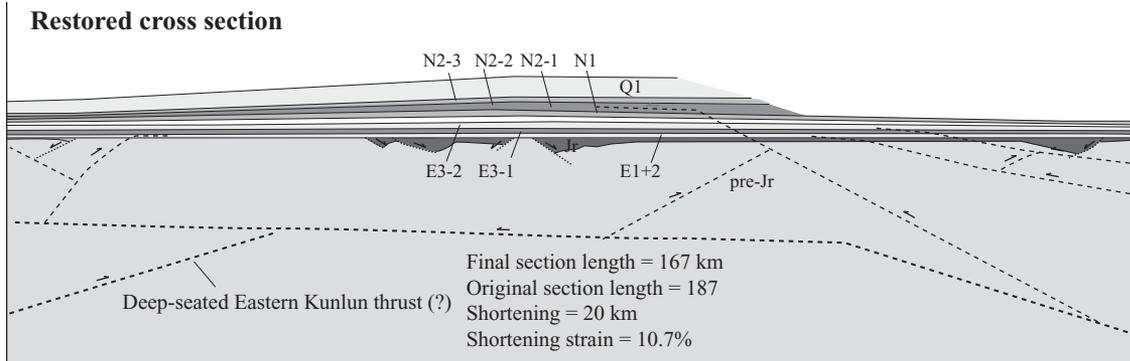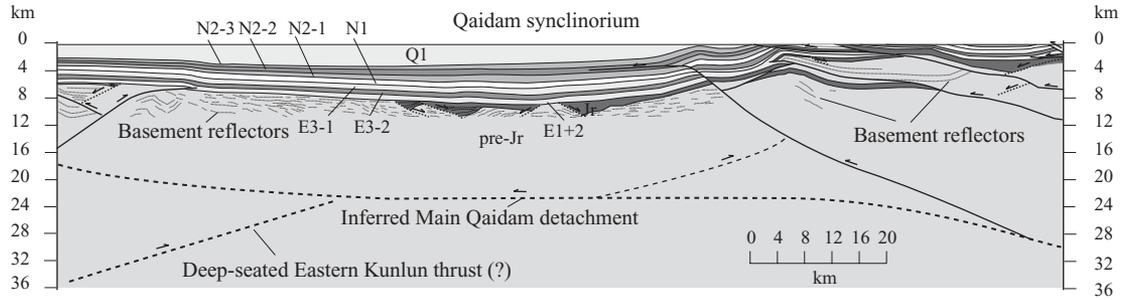
Figure 8. Geologic cross section of line 4 (upper diagram) and the restored section (lower diagram). See Figure 3 for location. The total amount of shortening is 20 km, with a shortening strain of 11%. Jr—Jurassic. See Table 1 for definition of lithologic units.
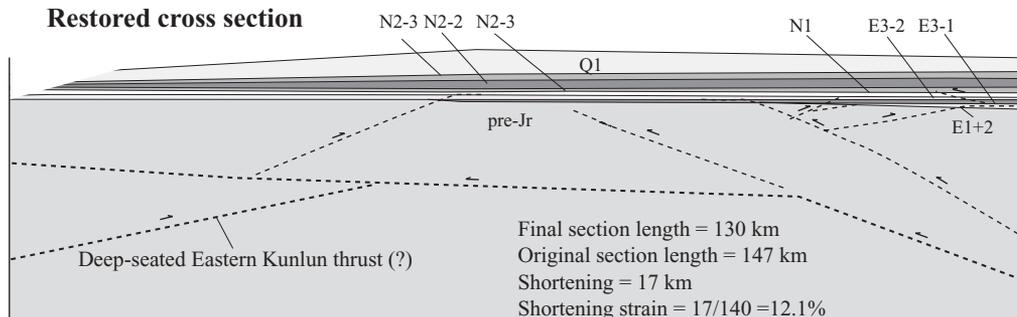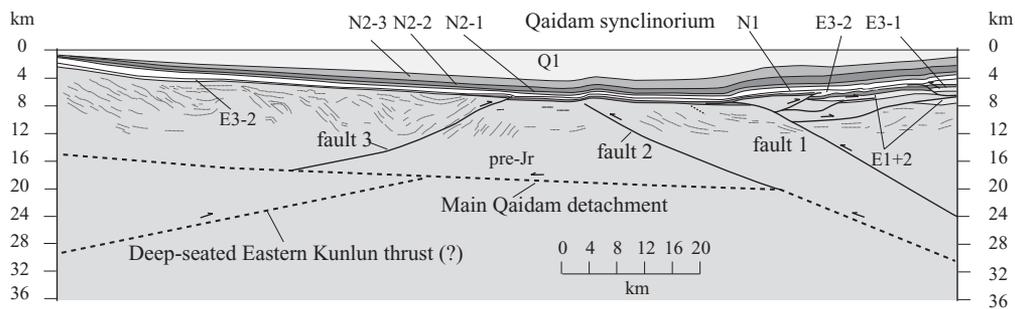

Figure 9. Geologic cross section of line 5 (upper diagram) and the restored section (lower diagram). See Figure 3 for location. The total amount of shortening is 17 km, with a shortening strain of 12%. Jr—Jurassic. See Table 1 for definition of stratigraphic units.

ramp linking the Main Qaidam detachment at its northern and southern ends is missing. This may be explained by the upper-crustal ramp located below the Eastern Kunlun Range outside the section.

Growth-Strata Relationships and Timing of Deformation

At this section younger Paleogene units progressively overlap underlying older unit southward (Fig. 9), suggesting southward expansion of deposition in the Qaidam basin. The generally northward thickening of units E1+2, E3–1, and E3–2 is indicative of a foreland basin bounded by a north-dipping thrust along the northern Qaidam margin. The inferred thrust is exposed at the surface as the north-dipping Xitie Shan thrust (Fig. 3) (Yin et al., 2008). Unit N1 (29–24 Ma) thickens slightly toward the northern and southern margins of the basin, suggesting that Qaidam basement was warped upward during its deposition. Unit N2–1 (24–10 Ma) shows little variation in thickness, whereas units N2–2 (10–5 Ma) and N2–3 (5–2 Ma) display gradual northward thickening, suggesting the basin was progressively tilting northward during deposition of these units. Unit Q1 thickens at the core of the synclinorium, indicating that the Qaidam synclinorium was developed in the past 2–1 m.y. and remains active. Except unit Q1, all other Cenozoic units maintain their thickness across the triangle zone in the northern Qaidam basin. Thus, the development of that triangle zone must have started in the Quaternary coeval with formation of the Qaidam synclinorium.

In summary, the growth-strata relationships in section 5 indicate five stages of basin development: (1) protracted northward tilting at 65–29 Ma, (2) upward warping between 29 and 24 Ma, (3) no basin tilting or detectable deformation between 24 and 10 Ma, (4) resumed northward tilting between 10 and 2 Ma, and (5) formation of the Qaidam synclinorium and the triangle zone in the northern Qaidam basin in the past 2 m.y.

Strain and Strain Rate

The total amount of shortening is 17 km, which yields a total shortening strain of 12%. The magnitude of shortening is relatively small compared to those estimated for sections 1–4. However, the duration of deformation that generated most of the observed shortening is only ~2 m.y., which yields a rather fast strain rate of 3.2×10^{-15} s^{-1}.

Mesozoic Structures

Jurassic strata are completely absent in section 5. Because Paleocene and Eocene units

E1+2 and E3–1 are pinched out in the northern part of the section, it is possible that Jurassic strata were originally deposited in the northern part of the section but were later eroded away during northward tilting of the basin.

Interpreted Seismic Section 6

Structural Geology

This section is ~110 km east of section 5 and extends into the southernmost part of the Qilian Shan–Nan Shan thrust belt (Fig. 10). Along this section the Qaidam basin is bounded in the north by the north-dipping Aimunik frontal thrust and in the south by a north-dipping unconformity. The slip magnitude of the Aimunik frontal thrust is ~6 km. The southern section displays a minor south-dipping thrust system (Huobuxun thrust system) with a total fault slip <2 km. The basin floor dips ~5° to the north. The small fault slip across the Huobuxun thrust system cannot explain the northward tilt of the southern Qaidam basement (Fig. 10). Thus, we suggest that the tilt was induced by thrust loading due to motion on the Aimunik frontal thrust. It is also possible that the northward tilting was caused by a deep-seated south-dipping thrust below the southern Qaidam basin (Fig. 10). Other mechanisms such as channel flow or distributed ductile shortening in the lower crust are also possible (see discussion below).

Growth-Strata Relationships and Timing of Deformation

In the northern margin of the Qaidam basin, the north-dipping basin-bounding fault system started to develop after deposition of unit N2–1 (Fig. 10). This is indicated by the presence of units N2–2 and N2–3 in the footwall and their absence in the hanging wall of the Aimunik frontal thrust. Although most Cenozoic units exhibit a southward transgressional relationship, unit N1 is an exception that shows a northward regressional relationship. This observation may be explained by an increase in sediment supplies to a northward-sloping foreland basin during deposition of unit N1. Alternatively, the regressional relationship for unit N1 could be attributed to motion on the northern branch of the Huobuxun thrust system (fault 1 in Fig. 10), which was associated with the development of a fault-propagation fold above and deposition of growth strata over its forelimb. Motion on fault 1 and the development of the fault-propagation fold may have eroded unit N1 over the crest of the anticline, resulting in its southward pinch-out geometry. This interpretation implies that deformation across the Huobuxun thrust system occurred after the end of the late Oligocene (i.e., after ca. 24 Ma).

Because there is no change in bed thickness across fault 2 in the Huobuxun thrust system, motion on fault 2 must have started after deposition of unit E3–2. However, it is not clear whether units N2–1 to N2–3 were deposited prior to motion on fault 2 and were subsequently eroded away, or if they were only deposited in the footwall of the fault. The first scenario implies that the fault started to move after deposition of unit N2–3 (i.e., the Pliocene), while the second scenario requires that the fault initiated during deposition of unit N2–1 (early to middle Miocene). In any case, the above observations suggest that deformation in section 6 started at or after the early Miocene (ca. 24 Ma).

Strain and Strain Rate

The shortening strain is highly inhomogeneous in the section. Shortening across the southern part of the section in the Qaidam basin proper is only ~2 km, which yields a shortening strain <1%. In contrast, shortening in the northern part of the section across the basin-bounding structures (i.e., the Aimunik thrust zone) is ~12 km, which yields a 30% strain. Using 24 m.y. as the duration of deformation, the average strain rate along line 6 is 0.13×10^{-16} s^{-1}.

Mesozoic Structures

Jurassic strata generally maintain a constant thickness in the northern part of the section, but they pinch out with Cenozoic units E3–2 to N2–3 at the southern part of the section, and were overlain by Quaternary deposits (Fig. 10). This relationship suggests that erosion of the Jurassic strata occurred in the Cenozoic, possibly resulting from northward tilting of the Eastern Kunlun Range that bounds the Qaidam basin. An extensional fault with ~2 km normal separation and an associated half-graben are present in the southern part of the section.

Interpreted Seismic Section 7

Structural Geology

This section traverses the southern part of the Yousha Shan anticline in the southwestern Qaidam basin (Fig. 11). The structural geometry and kinematic evolution of the anticline were discussed in detail in Yin et al. (2007a). Here we expand that study by considering an additional seismic reflection profile west of the sections discussed by Yin et al. (2007a) and Song and Wang (1993) (Fig. 3). Section 7 mainly exhibits two sets of thrusts: (1) south-dipping thrusts in the southern part of the section placing the pre-Jurassic basement over Neogene strata, and (2) north-dipping thrusts in the northern section placing pre-Jurassic basement over Paleogene strata and structurally below the south-dipping
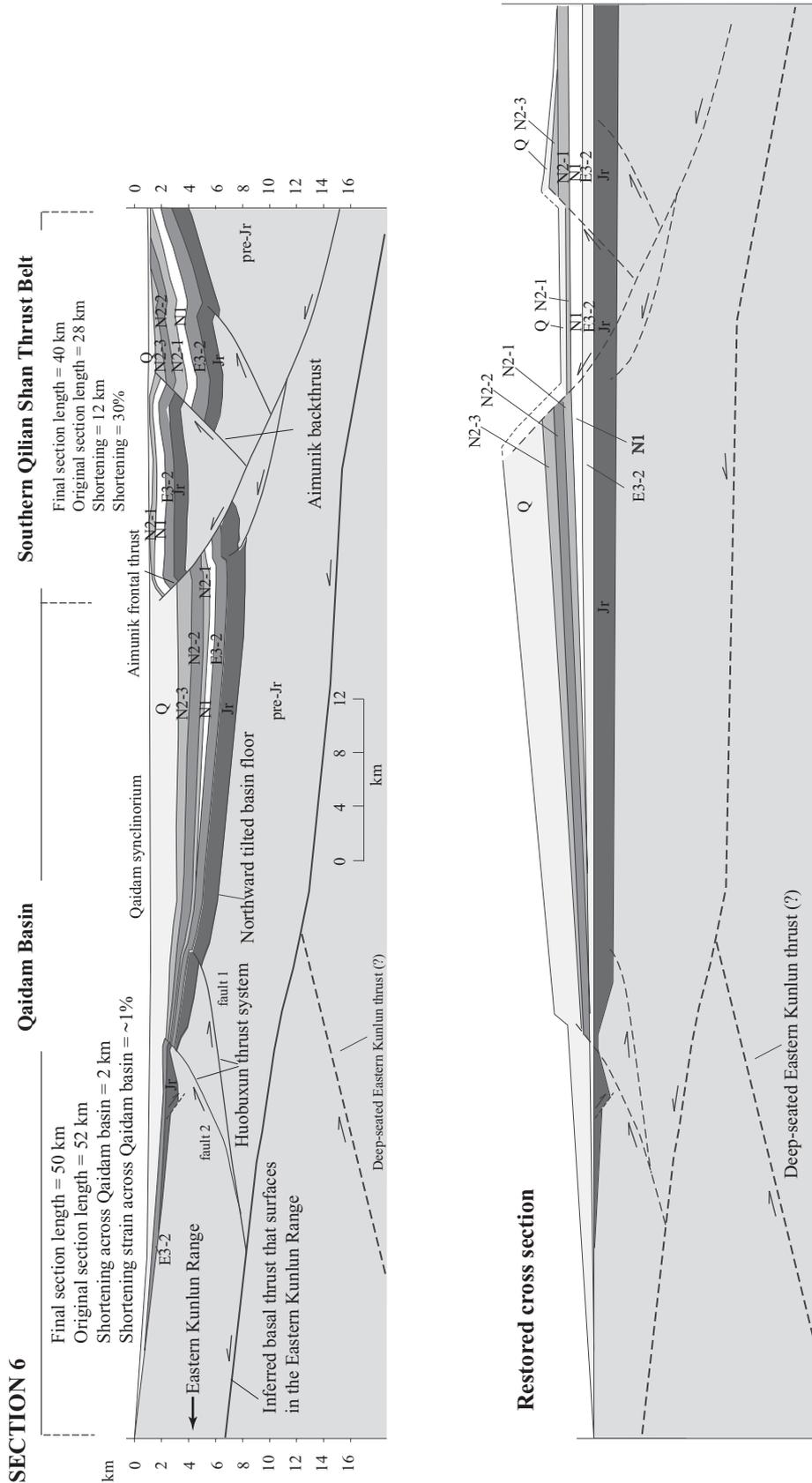
Figure 10. Geologic cross section of line 6 (the upper diagram) and the restored section (lower diagram). See Figure 3 for location. This section crosses the boundary between the Qaidam basin and southern Qilian Shan thrust belt. The total amount of shortening across the basin is ~2 km, which yields a shortening strain of ~1% over an original section ~52 km long. In contrast, the amount of shortening across the southern Qilian Shan thrust belt is 30% (i.e., 12 km shortening over a 40 km original section length). Jr—Jurassic. See Table 1 for definition of stratigraphic units.
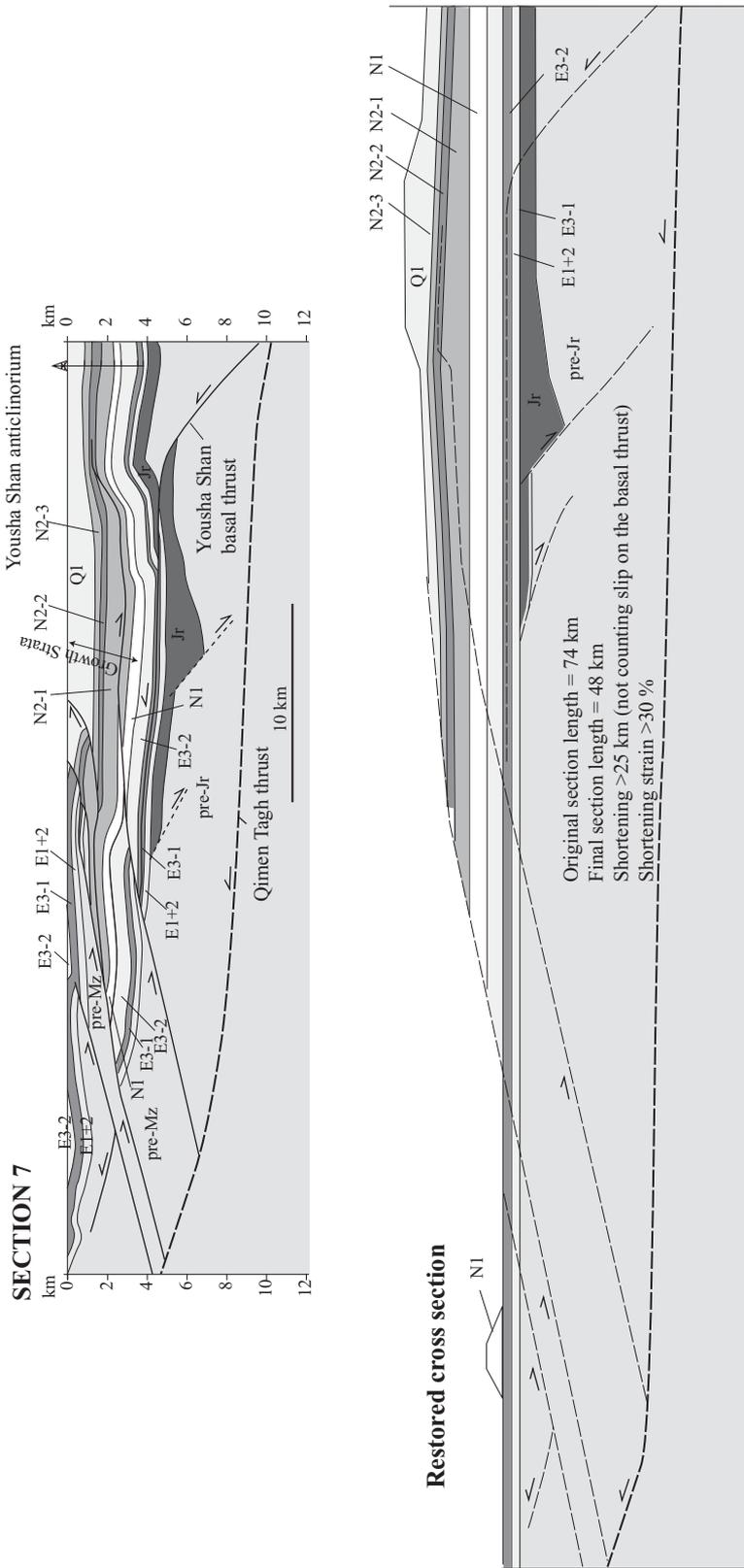
SECTION 7

Yousha Shan anticlinorium

Yousha Shan basal thrust

Qimen Tagh thrust

10 km

Restored cross section

Original section length = 74 km
Final section length = 48 km
Shortening >25 km (not counting slip on the basal thrust)
Shortening strain >30 %

Figure 11. Geologic cross section of line 7 (the upper diagram) and the restored section (lower diagram). See Figure 3 for location. The total amount of shortening is >25 km (not counting slip on the basal thrust), with a shortening strain of >30%. See Table 1 for definition of stratigraphic units. Note that units N2-1 and Q are prominent growth-strata sequences, whereas N2-2 and N2-3 maintain constant thickness. This relationship suggests that the Yousha Shan anticline was active episodically: active deformation during deposition of units N2-1 and Q with an intervening period of inactivity during deposition of units N2-2 and N2-3.

thrusts. Both fault sets may sole into a common décollement linked with south-directed thrusts in the Qimen Tagh Range to the south (Yin et al., 2007a) (Fig. 2).

Growth-Strata Relationships and Timing of Deformation

A growth-strata sequence is developed over the forelimb of the Yousha Shan anticline, which started during deposition of unit N1 (29–24 Ma) and became most prominent during the deposition of Quaternary strata (Fig. 11). This relationship indicates that the initiation of the Yousha Shan anticline occurred in the late Oligocene and the structure has remained active. A similar conclusion on the initiation age of deformation in the Yousha Shan region was reached by Yin et al. (2007a), based on reinterpretation of a seismic section by Song and Wang (1993) (see Fig. 3 for line location).

Strain and Strain Rate

The total amount of crustal shortening across section 7 is ~25 km, not counting slip on the inferred Qimen Tagh basal thrust. This yields ~30% shortening strain. This shortening strain is smaller than that estimated from a longer cross section to the east (Yin et al., 2007a), which yields a minimum shortening strain of 48%. This discrepancy can be explained by the different coverage of the two sections. The cross section of Yin et al. (2007a) extends across the entire Yousha Shan anticline and covers two additional major structures to the north: the north-dipping Yiematan and Chaishiling thrusts. In contrast, section 7 is much shorter and only covers the forelimb of the Yousha Shan anticline. Thus, we consider the estimated >48% shortening strain from Yin et al. (2007a) to be more representative of the overall shortening across the southwestern part of the Qaidam basin. The average shortening strain rate over a period of 29 m.y. (i.e., since the late Oligocene) is 5.1×10^{-16} s^{-1}.

Mesozoic Structures

Jurassic strata are restricted to the northern part of the section (Fig. 11). Two north-dipping normal-separation faults are present in the section. The southern fault has >~1.5 km normal separation and the northern fault has ~2 km normal separation. Half-grabens are associated with both faults (Fig. 11).

CENOZOIC SEDIMENTATION

In order to elucidate the Cenozoic development of the Qaidam basin, we summarize below the thickness-distribution history of Cenozoic strata in eight time slices (Fig. 12). The main data source is Huang et al. (1996), who

compiled information from more than 1000 drill holes and a dense network of seismic profiles. We modify their maps across our sections where appropriate. To highlight the first-order depositional patterns, we also remove the effect of thrusts on isopachs (Fig. 12). This simplification has little impact on the thickness distributions because major thrusts tend to concentrate along the basin margins and the largest fault slips tend to be localized in the Jurassic strata or basal part of the Cenozoic section such as in the North Qaidam triangle zone.

Early Eocene (E1+2, Lulehe Formation)

The east-west extent of the Paleocene–early Eocene Qaidam basin is much smaller than its present size, with its eastern boundary located west of Golmud (Fig. 12A). The largest depocenter for unit E1+2 is located in the northwestern basin (subbasin A in Fig. 12A), occupying an area of 150 km × 70 km. The thickest part of the depocenter is located ~80 km south of the present-day northern basin margin. Four smaller depocenters are also scattered in the northern Qaidam basin. The structural setting of the above depocenters can be understood by examining the northern parts of sections 1, 2, and 3, in which the thickest and largest depocenter (subbasin A) is located in the core of the Qaidam synclinorium, whereas the smaller depocenters are located in over smaller synclines. Two minor depocenters are located in the southern Qaidam basin (subbasins B and C in Fig. 12A): one near Yousha Shan anticline (subbasin B) and the other in the south-central Qaidam basin (subbasin C). The latter is located in the core of a small syncline (Fig. 7), whereas the origin of the former is not clear due to lack of seismic data in the area complex. Several short-wavelength (<30 km), shallow (<500 m), and circular subbasins were developed along the eastern margin of the basin.

Middle to Late Eocene (E3–1, Lower Xiaganchaigou Formation)

During deposition of unit E3–1, subbasins A, B, and C became larger (Fig. 12B). This is associated with an overall eastward expansion of the Qaidam basin, with its new eastern boundary located east of Golmud. The center of subbasin A also migrated southward, occupying the central position of the Qaidam basin. The most noticeable change at this time is the increase in the north-south width of subbasin A. This increase is associated with a coeval increase in the amplitude and wavelength of the underlying Qaidam synclinorium (Fig. 13). Subbasins B and C also expanded laterally. The small

subbasins along the eastern margin of the Qaidam basin similarly became larger (wavelength >50 km) and more elongated compared to the E1+2 pattern (Fig. 12A; cf. Fig. 12B).

Early Oligocene (E3–2, Upper Xiaganchaigou Formation)

During deposition of unit E3–2, subbasins A, B, and C all expanded in the northeast and southwest directions perpendicular to the structural trend in the basin (Fig. 12C). The most prominent feature is the appearance of a southward-thickening subbasin D near Golmud, which may be controlled by the presence of a north-directed thrust to the south. Subbasin C also became more asymmetric, with the north-dipping slope on the south side steeper than the south-dipping northern slope on the north side (Fig. 12C). The extent of unit E3–2 is approximately the same as that of the current Qaidam basin. Subbasins on the east side became much more elongated, as expressed by the development of two rows of northwest-trending troughs (Fig. 12C).

Late Oligocene (N1, Shangganchaigou Formation)

The main feature of the N1 isopach pattern is that subbasin A became larger by incorporating subbasin C and part of subbasin B developed earlier (Fig. 12D). Subbasin D, which was prominent during deposition of unit E3–2, is completely absent. Subbasin B is partitioned into western and eastern basins (B-west and B-east), with subbasin B-east joining the larger subbasin A (Fig. 12D). In addition to the continuous enlargement of subbasin A, two smaller subbasins (A-1 and A-2) are present along the northwestern margin of the Qaidam basin. In the eastern half of the basin, the isopach pattern is simplified, as expressed by one asymmetric basin with a gentle southern slope and a steep northern slope (Fig. 12D).

Early and Middle Miocene (N2–1, Xiayoushashan Formation)

The depositional pattern of unit N2–1 is similar to that for unit N1 (Fig. 12E). Key differences are the disappearance of subbasins A-1 and A-2 shown during deposition of unit N1. An asymmetric subbasin remains in the eastern half of the basin.

Late Miocene (N2–2, Shangyoushashan Formation)

During deposition of unit N2–2, a northwest-trending synclinal trough extending from sub-

basin A through subbasins C, E, F, G, and F was developed (Fig. 12F). This synclinal trough was built on an earlier structural arch in the eastern Qaidam basin, which became converted into a series of small basins (i.e., subbasins E, F, G, and H). Meanwhile, subbasins A, B, and C in the western Qaidam basin continued to develop.

Pliocene (N2–3, Shizigou Formation)

During deposition of unit N2–3, the depocenter of subbasin A migrated prominently to the east for ~100 km, leaving behind a small subbasin occupying its original depocenter during deposition of unit N2–2 (Fig. 12G). In the eastern half of the Qaidam basin, the isopach data show that the broad synclinal trough continued to develop, with a gentler slope in the south and a steeper slope in the north. In contrast, the western half of the Qaidam basin is characterized by numerous short-wavelength (<40 km) and shallow (mostly <500 m) basins (Fig. 12G).

Quaternary (Q, Qigequan Formation)

The isopach pattern of Quaternary deposits reflects the modern depositional system across the Qaidam basin (Fig. 12H). The main depocenter lies along the northwest-trending basin axis, with sediments fed mainly by internally drained rivers from the Eastern Kunlun Range to the south. The highly elongated troughs and arches are correlative with active growing anticlines and synclines (Fig. 13).

DISCUSSION

Tectonic Origin of Qaidam Basin

Our results on the timing, style, and magnitude of Cenozoic deformation across the Qaidam basin are summarized in Figures 13 and 14A. This information allows us to evaluate the existing tectonic models for the development of the Qaidam basin. The diachronous initiation of deformation and the lack of strike-slip faults along the northern and southern basin margins (also see Yin et al., 2008, 2007a) preclude extrusion of the Qaidam basin from the west (Wang et al., 2006) (Fig. 13). The older initiation age of deformation in the northern basin margin ca. 65–50 Ma and the younger initiation age of deformation in the southern basin margin at 29–24 Ma are inconsistent with the stepwise northward-jumping model (Métivier et al., 1998). As shown in Figure 13, our structural observations are consistent with the suggestions that a basement-involved thrust belt lies across the Qaidam basin (Burchfiel et al., 1989), and the first-order structure of the
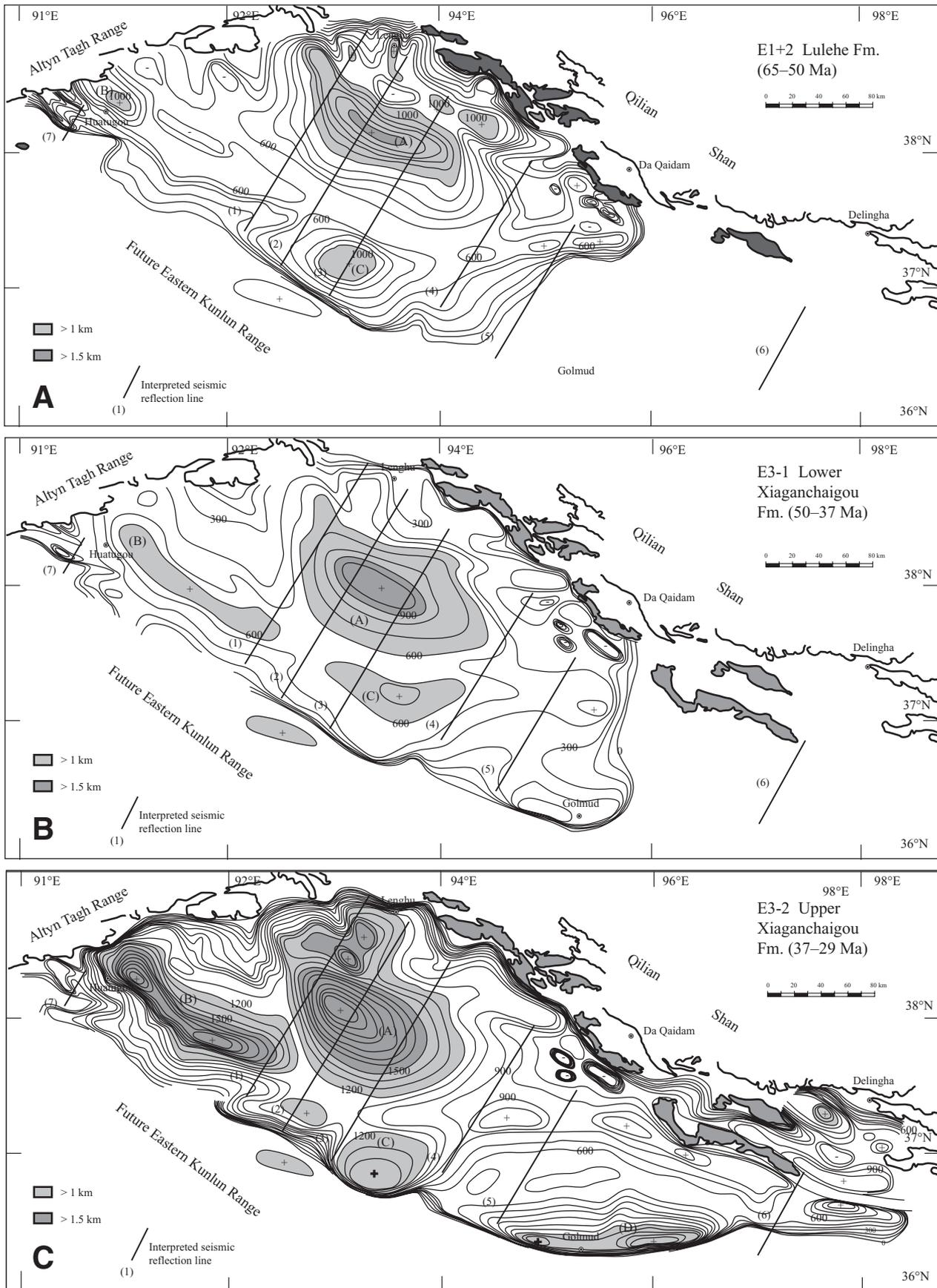
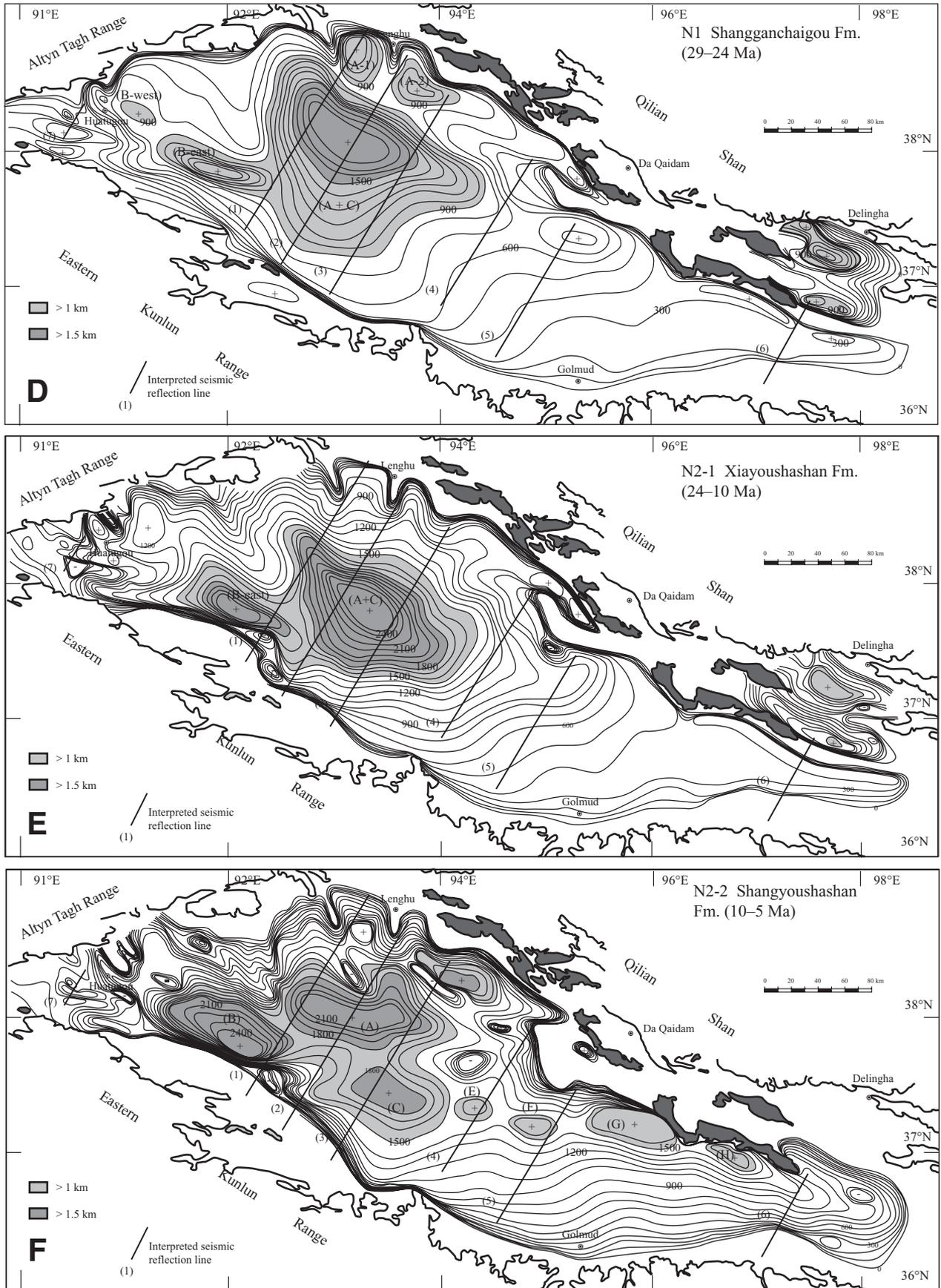**Figure 12** (*Continued on following page*).

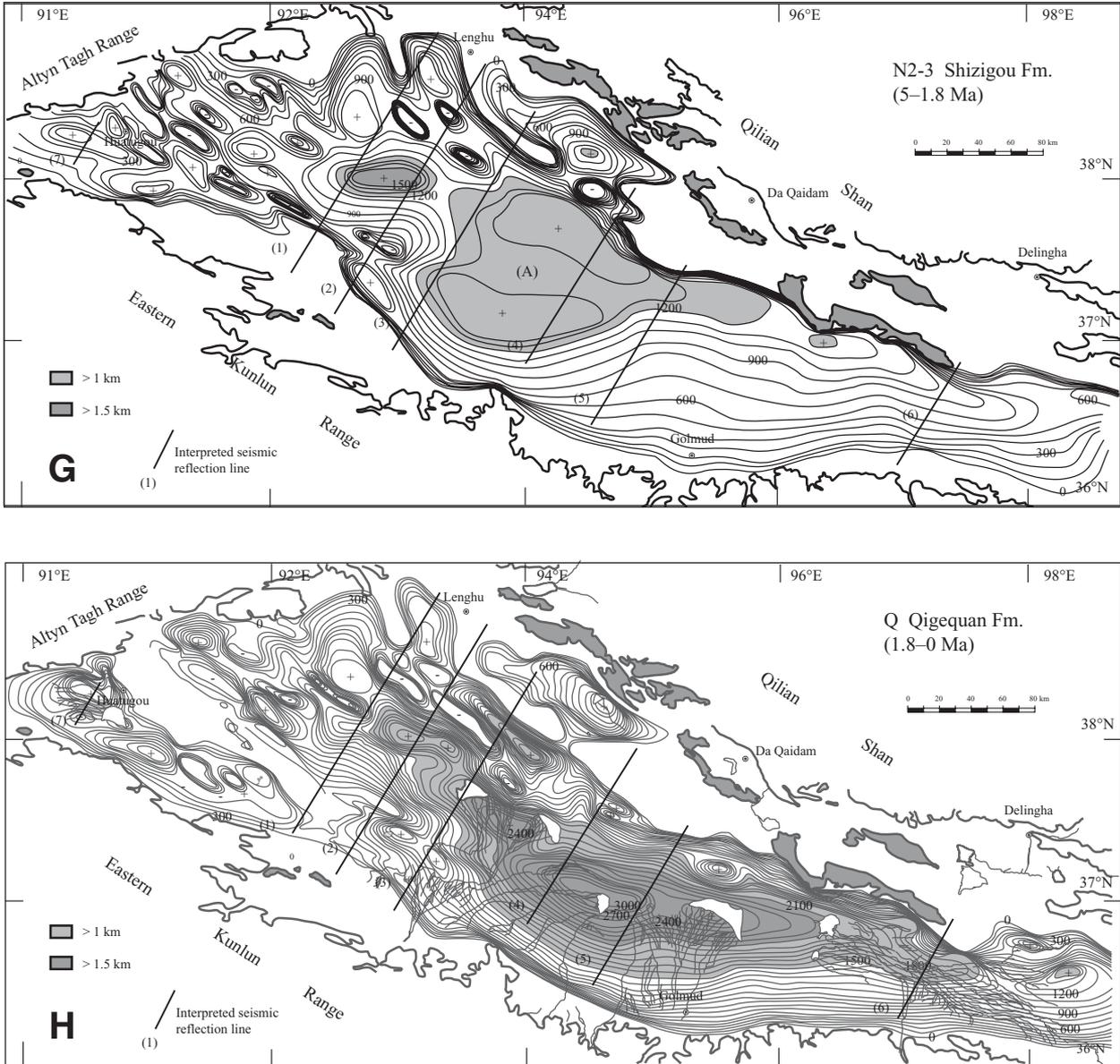**Figure 12** (*Continued on following page*).

Figure 12 (*continued*). (A) Isopach map of the Lulehe Formation (E1+2). (B) Isopach map of the lower Xiaganchaigou Formation (E3-1). (C) Isopach map of the upper Xiaganchaigou Formation (E3-2). (D) Isopach map of the Shangganchaigou Formation (N1). (E) Isopach map of the Xiayoushashan Formation (N2-1). (F) Isopach map of the Shangyoushashan Formation (N2-2). (G) Isopach map of the Shizigou Formation (N2-3). (H) Isopach map of Quaternary sediments (Q). See Table 1 for age assignment of each unit.
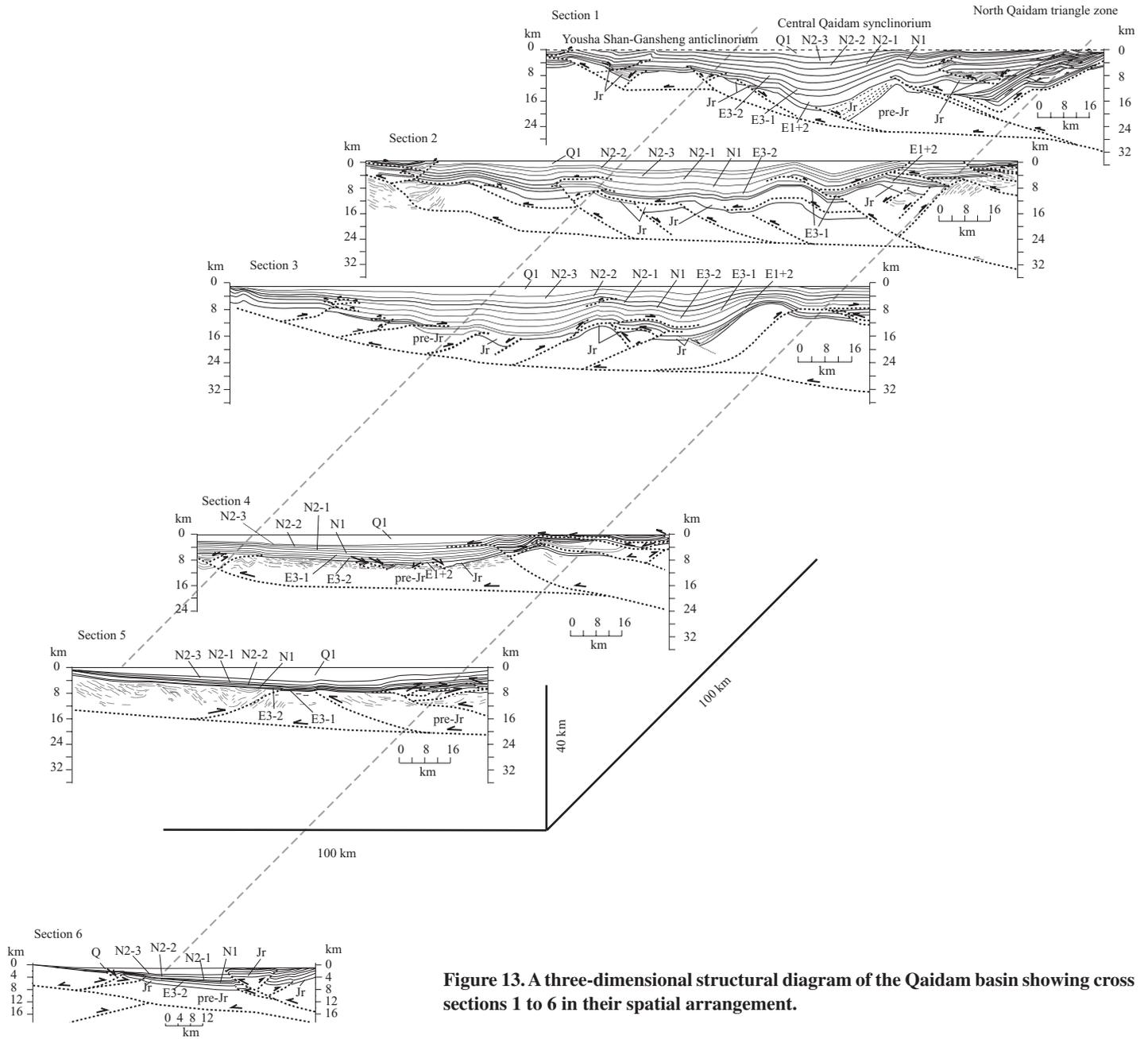
Figure 13. A three-dimensional structural diagram of the Qaidam basin showing cross sections 1 to 6 in their spatial arrangement.
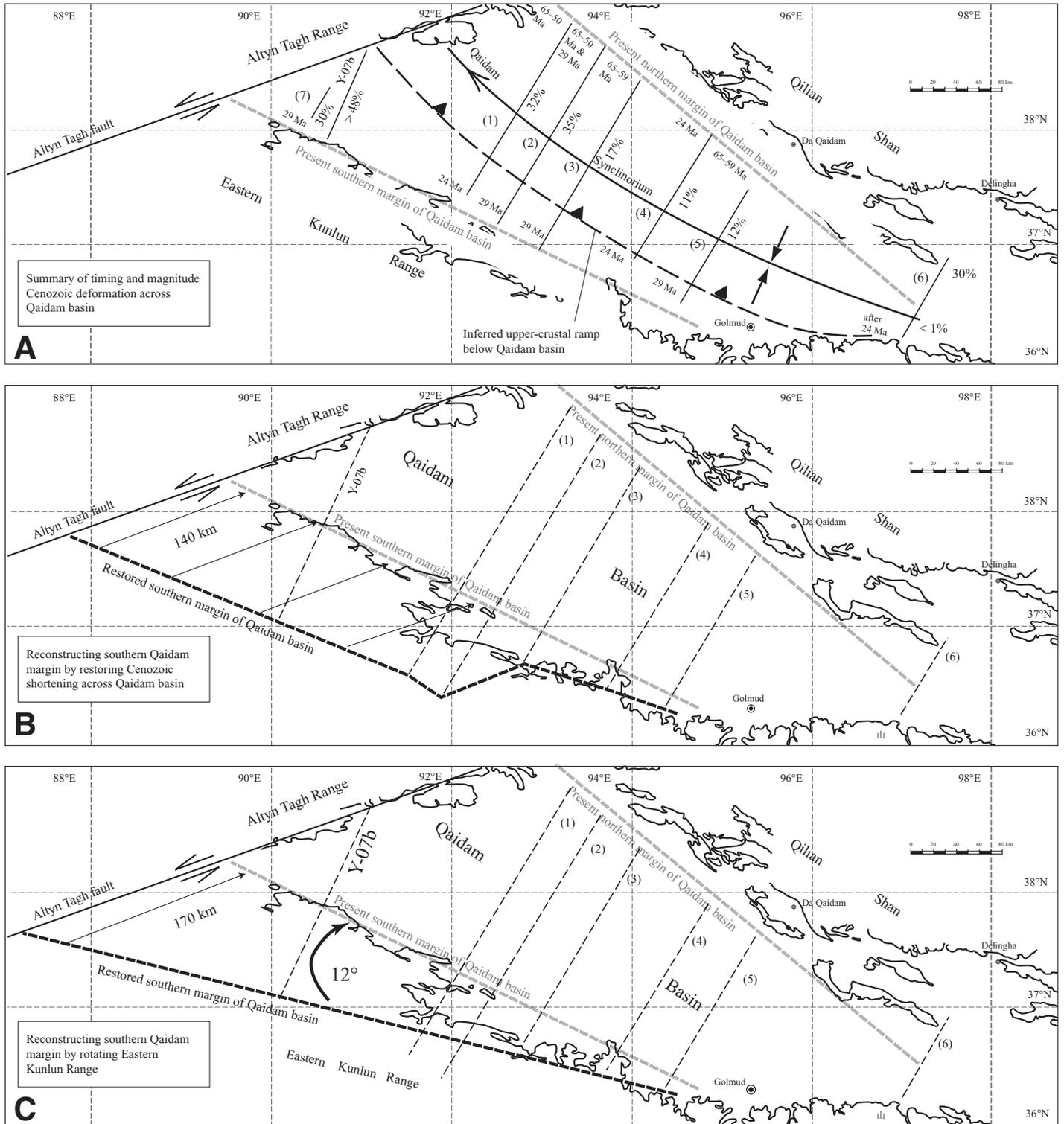
Figure 14. (A) Summary of timing and shortening strain across the Qaidam basin. (B) Reconstruction of southern Qaidam margin relative to its northern margin by projecting the magnitude of shortening along the western edge of the Qaidam basin against the Altyn Tagh fault. This projection predicts ~140 km shortening across the western edge of the Qaidam basin along the Altyn Tagh fault. (C) Restored southern margin of the Qaidam basin by rotating the Eastern Kunlun Range 12° in a clockwise sense. This projection predicts ~170 km shortening along the western edge of the Qaidam basin against the Altyn Tagh fault.

Geologic time		Age (Ma)	Southern Qaidam Basin			Hoh Xil Basin		
			Units	*Thickness (m)*	*Facies*	*Units*	*Thickness (m)*	*Facies*
PLIO			Shizigou Formation	>1500	Lacustrine			
MIOCENE	Late	—10	Shangyou-shashan Fm.	>822	Lacustrine			
	Middle		Xiayousha-shan Fm.	1243	Lacustrine/ fluvial			
	Early	—20				Wudaoliang Group	370	Lacustrine
OLIGOCENE	Late		Shanggan-chaigou Fm.	848	Fluvial/ lacustrine	missing or no depsitional records		
	Early	—30	Lower and Upper Xiagan-chaigou Fm.	1011	Fluvial/ lacustrine	Yaxicuo Group	670	Fluvial/lacustrine
EOCENE	Late	—40				Fenghuo Shan Group	4790	Fluvial/lacustrine/ fan-delta
	Middle							
	Early	—50	Lulehe Formation	1043	Alluvial/ fluvial			
PALEOCENE	Early	—60				*Underlying Jurassic and Cretaceous strata*		

Figure 15. Comparison of Cenozoic stratigraphy of the southern Qaidam basin after Song and Wang (1993) and the Hoh Xil basin after Liu et al. (2001, 2003). See text for detailed discussion.

limestone started ca. 26 Ma and was coeval with the initial uplift of the Eastern Kunlun Range at 30–20 Ma (Mock et al., 1999; Jolivet et al., 2001, 2003; Yuan et al., 2006). This temporal correlation can be explained by the uplift of the Eastern Kunlun Range that caused partitioning of the once-connected Hoh Xil and Qaidam basins in central Tibet, which we refer to as the Paleo-Qaidam basin (Fig. 1). The uplifted Eastern Kunlun Range acted as a dam, trapping sediments in the Hoh Xil basin in the Miocene.

Following the above explanation, we propose a simple scheme for the development of the Qaidam basin in the context of the overall evolution of the Tibetan plateau. In the Paleocene–early Eocene, collision-induced stress reactivated the early Paleozoic Qilian orogen in the north (Jolivet et al., 2001; Yin et al., 2002, 2008; Dupont-Nivet et al., 2004; Horton et al., 2004; Sun et al., 2005; Zhou et al., 2006) and the Late Triassic Jinsha suture zone (Coward et al., 1988; Dewey et al., 1988; Yin and Harrison, 2000; Horton et al., 2002; Spurlin et al., 2005) in the south; this process created the Qilian Shan–Nan Shan and Fenghuo Shan thrust belts with a large topographic depression in between. Paleogene deformation bypassed the Lhasa block that had already been elevated in the Cretaceous (Yin et al., 1994; Murphy et al., 1997) (Figs. 2 and 16A). Thickened crust in the Qilian Shan and Eastern Kunlun Shan also directed collision-induced stress to exploit the preexisting weakness, the Triassic Kunlun suture. This has led to Neogene development of the left-slip Kunlun fault and the kinematically linked Qimen Tagh and Bayanhar thrust belts (Kidd and Molnar, 1988; Jolivet et al., 2001, 2003; Yuan et al., 2006; Yin et al., 2007a) (Fig. 16B).

Paleogene crustal thickening of the northern Tibetan plateau may have also caused stress propagation across the Tarim basin to reactivate the late Paleozoic Tian Shan orogen and to form a new thrust belt beginning since the late Oligocene (ca. 26–24 Ma) (Windley et al., 1990; Avouac et al., 1993; Yin and Nie, 1996; Yin et al., 1998). The Tian Shan uplift in turn partitioned the once-connected Tarim and Junggar basins (Fig. 16). Currently the Tarim basin is in an initial stage of disintegration, being consumed by thrusting around its rims and inside its interior; the latter is expressed by the development of the Maza Tagh thrust system (Kang, 1996; Jia, 1997) (Fig. 16B). If the Indo-Asian collision continues for the next 54–60 m.y., the approximate life span of the current Tibetan plateau (Yin and Harrison, 2000), the Tarim basin will eventually be incorporated into the Tibetan plateau and the Altyn Tagh fault will be entirely inside the expanded plateau, like the Kunlun fault today (Figs. 1 and 16).
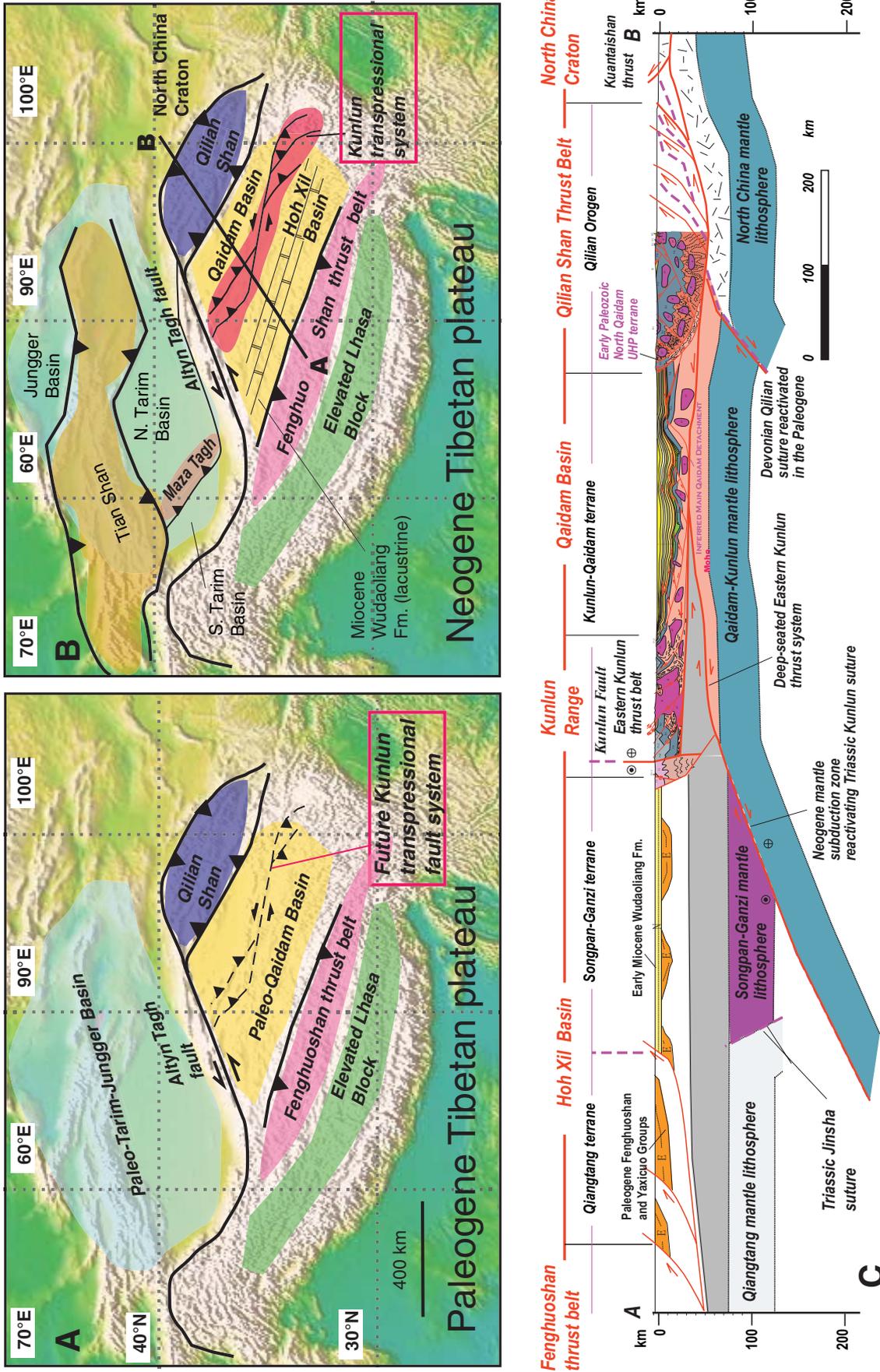
basin is characterized by a large synclinorium (Bally et al., 1986).

How the Qaidam basin has evolved from its inception to its present form has important implications for understanding the overall development of the Tibetan plateau. All existing models for the development of the Qaidam basin predict the basin to have the same bounding structures since its initial formation (e.g., Bally et al., 1986; Métivier et al., 1998; Wang et al., 2006). This inference is inconsistent with the timing of deformation across the Qaidam basin obtained from this study and the uplift history of the Eastern Kunlun Range determined by early workers. As shown above, synchronous sedimentation occurred across the entire western Qaidam basin at 65–50 Ma, coeval with the initiation of the northern basin-bounding structures. However, the southern basin-bounding structures did not start until after 29–24 Ma. Existing thermochronologic data indicate that the uplift of the Eastern Kunlun Range occurred after 30–20 Ma (Mock et al., 1999; Jolivet et al., 2001, 2003; Wang et al., 2004; Liu et al., 2005; Yuan et al., 2006). The above observations suggest that the Paleocene–early Oligocene Qaidam basin may have

extended much farther south across the Eastern Kunlun Range, which did not exist during this time interval. This leads to the possibility that the Paleogene Qaidam basin in the north and the Hoh Xil basin of Liu et al. (2001, 2003) in the south were once parts of a single topographic depression spanning >500 km in the north-south direction (i.e., one-third of the 1500-km-wide Tibetan plateau) (Fig. 1).

Linking tectonic evolution of the Qaidam basin with Cenozoic uplift history of the Eastern Kunlun Range helps explain the long noted two-stage development of the Hoh Xil basin and the related Fenghuo Shan thrust belt along the Triassic Jinsha suture (Leeder et al., 1988; Liu et al., 2001, 2003) (Fig. 1). The first stage involves the Eocene–Oligocene development of a foreland basin of the north-directed Fenghuo Shan thrust belt, as expressed by deposition of the dominantly alluvial and fluvial Fenghuo Shan Group (Fig. 15) (Liu et al., 2001, 2003). The second stage involves lacustrine deposition of the Miocene Wudaoliang Formation (mostly limestone) (Figure 15), which is flat-lying to gently folded over intensely folded Paleogene strata below (Leeder et al., 1988; Liu et al., 2001, 2003). The deposition of the Wudaoliang

Figure 16. (A) Paleogene tectonic configuration of the Tibetan plateau in present-day geographic coordinates. The Paleo-Qaidam basin lies between the elevated Lhasa block and the Fenghuo Shan thrust belt in the south and the elevated Qilian Shan in the north. The region north of the Tibetan plateau was a large topographic depression that links Tarim and Junggar basins across the Tian Shan, as the Tian Shan was not uplifted until the early Miocene. **(B)** Neogene tectonic configuration of the Tibetan plateau in present-day geographic coordinates. The initiation of the Eastern Kunlun left-slip transpressional system caused the uplift of the Eastern Kunlun Range, which has partitioned the Paleo-Qaidam basin into the Hoh Xil basin to the south and the Qaidam basin to the north. The uplift of the Tian Shan range similarly partitioned the once-united Tarim-Junggar basin into the Tarim basin to the south and Junggar basin to the north. The development of the Maza Tagh thrust zone in central Tarim basin is currently partitioning the Tarim basin into northern and southern subbasins. **(C)** Schematic cross section showing first-order crustal structures of the central and northern Tibetan plateau. Geology of the southern Qilian Shan is based on Yin et al. (2008), geology of the Qaidam basin is based on interpreted seismic section 3 in Figure 7, and geology of the Eastern Kunlun is based on our own unpublished mapping.

First-order lithospheric structures resulting from the above plateau-growth history are shown in Figure 16C. A question may be raised about our proposed Paleo-Qaidam basin hypothesis: why is the elevation of the Hoh Xil basin currently ~2 km higher than that of the Qaidam basin? Several mechanisms may have operated to cause this elevation difference in the Neogene once the two basins were partitioned. First, the high elevation of the Hoh Xil basin could have been induced by a thermal event in the mantle, such as convective removal of the Hoh Xil mantle lithosphere (e.g., Harrison et al., 1992; Molnar et al., 1993) or subduction of the Qaidam mantle lithosphere below the Hoh Xil region (e.g., Meyer et al., 1998; Yin et al., 2002). Second, it is possible that lower crust was extruded northward, as from the elevated Lhasa block into the Hoh Xil basin (e.g., Clark and Royden, 2000). Finally, it is possible that Hoh Xil lower crust was thickened by thrust duplication due to the development of a large flake-tectonics system across the Eastern Kunlun Range (Yin et al., 2008). The last hypothesis is consistent with our structural observations from the southwestern Qaidam basin, where excess lower crust must have been subducted below the nearby thrust belts (Yin et al., 2007a). The above end-member processes could have operated and interacted simultaneously, and more detailed geologic research is required across the Eastern Kunlun Range and the Hoh Xil basin to differentiate these possible mechanisms for plateau uplift.

The plateau-growth history proposed above implies that the largest plateau on Earth was constructed by first creating and then destroying large intracontinental basins. This view is in strong contrast to the passive-filling bathtub model of Métivier et al. (1998), Meyer et al. (1998), and Tapponnier et al. (2001) that invokes no crustal shortening once intraplateau basins were created. The proposed deformation sequence above (Fig. 16) is different from the predictions of the thin viscous sheet model or the continental extrusion model (England and Houseman, 1986; Tapponnier et al., 1982), as both require northward propagation of deformation across Tibet and eastern Asia. In contrast, models considering preexisting weakness and topography provide a better physical scheme to simulate the growth history of the Tibetan plateau (e.g., Neil and Houseman, 1997; Kong et al., 1997).

Deformation History and Basin-Forming Mechanisms

The Cenozoic deformation history of the Qaidam basin and associated sedimentation are illustrated in Figure 17. In the Paleocene and early Eocene, a triangle zone was developed along the northern edge of the Qaidam basin, and produced a southward tapering growth-strata sequence (Fig. 17B). The triangle zone continued to grow in the middle and late Eocene via development of a passive-roof thrust duplex, causing further thickening of the growth-strata sequence southward away from the triangle zone (Fig. 17C). In the late Oligocene and Miocene, the Qaidam synclinorium began to develop, caused by the formation of a south-directed thrust below the synclinal axis and a fault-bend fold along the southern Qaidam basin margin (Fig. 17D). The continuous development of the fault-bend fold from the Pliocene to the present in the southern Qaidam basin caused further tightening of the Qaidam synclinorium and deposition of a thick growth-strata sequence (Fig. 17E).

The most interesting observation from the Qaidam basin is its central axis has been persistently downgoing throughout the Cenozoic, with an amplitude locally reaching 16 km. In our kinematic model, we interpret it to have developed by the formation of two thrust systems initiated at different times below the two fold limbs. Although the development of crustal-scale folds by hidden thrust systems has been well documented in the North American Cordilleran fold-thrust belt (e.g., Price, 1981, 1986; Yin and Kelty, 1991), the folds are much smaller than those across the Qaidam basin (amplitude <5 km and half-wavelength <50 km). One possible explanation for the differences in fold size is that the North American Cordilleran thrust belt is thin-skinned, involving only the sedimentary cover sequence, whereas the Qaidam thrust belt is thick-skinned, involving even the lower-crustal basement. The diachronous initiation of the fold limbs across the Qaidam basin precludes buckling as a mechanism to grow the syncline (e.g., Cloetingh et al., 2002), although it could be the cause of initiation of the development of thrust duplexes (see experimental demonstration of this process by Burg et al., 1994). In addition to thrust loading by the development of thrust wedges on both sides of the Qaidam basin, it is also possible that additional forces have assisted downward warping of the basin axis. They may include the presence of a southward subducting lithospheric slab from the Qilian Shan–Nan Shan thrust belt or a downward drip of thickened lithosphere below the basin.

Classifying the Qaidam basin is not straightforward; its structural setting and isopach patterns differ from a classic foreland basin in that its main depocenter has been located persistently in the basin axis away from the bounding thrusts (Fig. 12) (e.g., Jordan, 1981). Alternatively, the Qaidam basin could be classified as a wedge-top basin in the sense of DeCelles and Giles (1996), lying above the Qimen Tagh–Eastern Kunlun thrust belt in the south and Qilian Shan–Nan Shan thrust belt in the north. Because the initiation age and structural style of the two thrust belts are significantly different, such a simple classification may obscure the complex basin history as illustrated by our reconstruction (Fig. 17). Naming the Qaidam basin as a simple piggyback basin suffers the same problem of oversimplifying the basin-forming process. Dickinson et al. (1988) noted that some latest Cretaceous–early Tertiary Laramide basins in the North American Cordillera were developed in hanging walls of large basement-involved thrusts, which they referred to as axial basins. Yin and Ingersoll (1997) found that these basins are commonly located in synclinal troughs above oppositely dipping thrusts. This structural setting in the broadest sense matches the tectonic setting of the Qaidam basin and its bounding thrust belts: the basis is bounded by the south-directed Qimen Tagh–Eastern Kunlun thrust belt in the south and the north-directed Qilian Shan–Nan Shan thrust belt in the north. The key difference between the North American and Tibetan axial basins is that the synclinal trough across the Qaidam region may be a lithospheric-scale fold.

Relationship between Deformation of the Qaidam Basin and Motion on the Altyn Tagh Fault

Results of our interpreted seismic sections and the earlier work in the westernmost Qaidam basin (Yin et al., 2007a) suggest that shortening strain and shortening magnitude across the Qaidam basin decrease systematically eastward: ~35% in the west, ~11% in the center, and <1% in the east (Fig. 14A). We used this information to reconstruct the original position of the southern Qaidam margin relative to the northern margin. In our reconstruction, we used the estimated strain of >48% (Yin et al., 2007a) for the westernmost part of the Qaidam basin (Fig. 14A). The restored southern basin margin requires ~140 km shortening across the westernmost the Qaidam basin and 140 km decrease in fault slip on the Altyn Tagh fault across the Qaidam basin (Fig. 14B): from ~470 km at its intersection with the southern Qaidam margin (Cowgill et al., 2003) to ~330 km at its intersection with the northern Qaidam margin. The eastward decrease in Qaidam shortening also implies that the southern Qaidam margin has rotated clockwise relative to its northern margin. If we treat the Eastern Kunlun Range as a rigid block, the along-strike variation of shortening requires >12° of clockwise rotation and
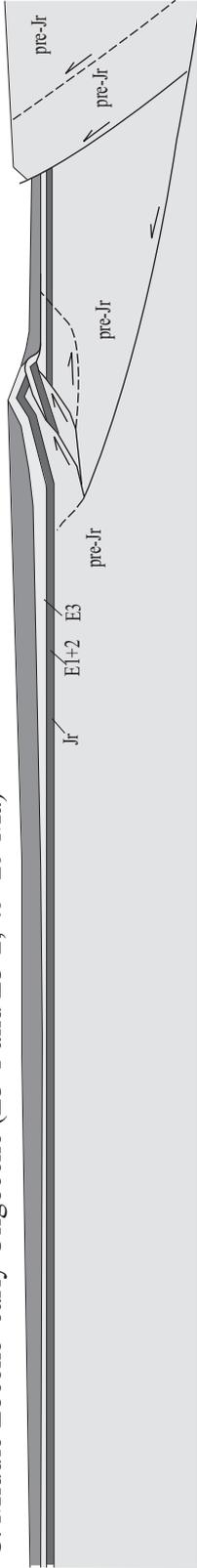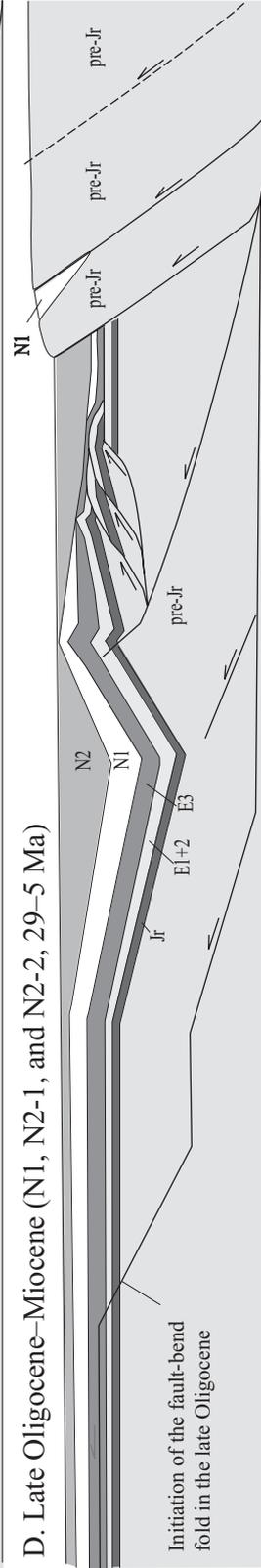
A. End of Cretaceous (ca. 65 Ma)
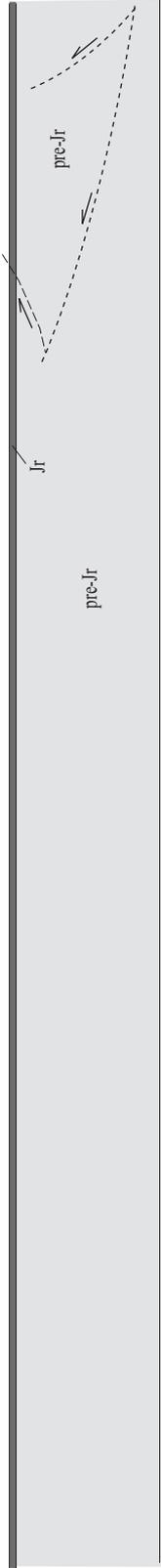
B. Paleocene–early Eocene (E1+2, 65–49 Ma)

C. Middle Eocene–early Oligocene (E3-1 and E3-2, 49–29 Ma)

D. Late Oligocene–Miocene (N1, N2-1, and N2-2, 29–5 Ma)

Initiation of the fault-bend fold in the late Oligocene

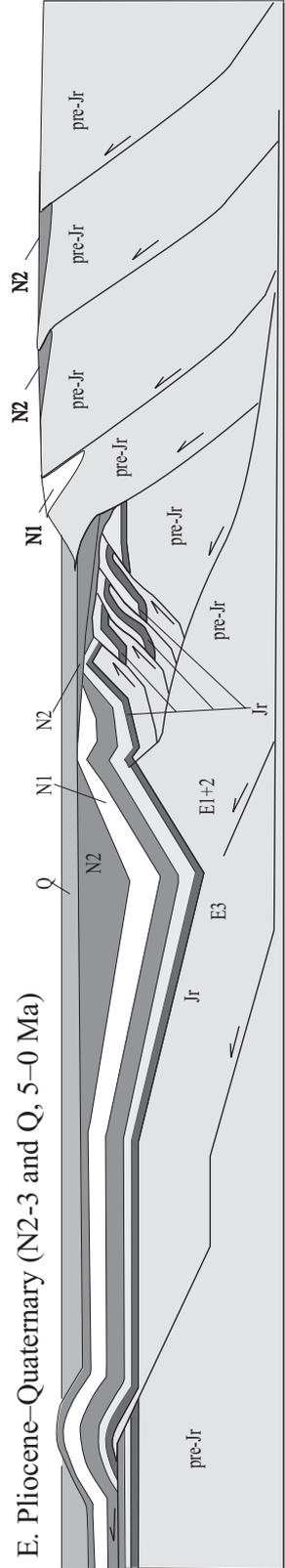E. Pliocene–Quaternary (N2-3 and Q, 5–0 Ma)

Figure 17. Restoration of cross section 1. Stage 1, end of Cretaceous (ca. 65 Ma); stage 2, Paleocene–early Eocene (E1+2, 65–49 Ma); stage 3, middle Eocene–early Oligocene (E3-1 and E3-2, 49–29 Ma); stage 4, late Oligocene–Pliocene (N1 and N2, 29–2 Ma); stage 5, Quaternary (2–0 Ma). Jr is Jurassic.

>170 km shortening across the westernmost the Qaidam basin; the slip magnitude on the Altyn Tagh fault is constrained to be <~300 km north of the Qaidam basin (Fig. 14C).

Our proposed tectonic rotation of the southern margin of the Qaidam basin relative to the northern basin margin can be tested by the existing paleomagnetic data across the basin. Paleomagnetic studies of middle Eocene–early Oligocene samples by Dupont-Nivet et al. (2002) along the northern margin of the Qaidam basin indicate that the region has not rotated with respect to the Eurasian reference pole since the early Oligocene (Fig. 2). A study of Cretaceous samples by Sun et al. (2006) at the eastern end of the Qaidam basin indicates that the region has not rotated in the Cenozoic (Fig. 2). In north-central Qaidam, Chen et al. (2002) showed that Paleogene red beds have rotated ~15° clockwise. Using Late Jurassic samples from the southwestern Qaidam basin, Chen et al. (2002) and Halim et al. (2003) showed that the region has rotated as much as ~29° clockwise prior to late Miocene; however, how much of this rotation occurred in the Cenozoic is not clear. In the Hol Xil region, samples from late Oligocene strata show that the region has rotated ~15° clockwise (Fig. 2). Liu et al. (2003) showed that in the Fenghuo Shan area of the Hoh Xil basin, the region has undergone 29° ± 8° of clockwise rotation since ca. 31 Ma (Fig. 2). The above data in general are consistent with our block rotation model and, in light of the paleomagnetic data from the Hoh Xil basin, our proposed 12° regional rotation of the Eastern Kunlun Range may represent a lower bound.

As we stated in Yin et al. (2008), we consider Cenozoic deformation across the Qaidam basin to have been driven by motion on the Altyn Tagh fault, as expressed by initiation of deformation and sedimentation at the western edge of the Qaidam basin against the Altyn Tagh fault and subsequent eastward propagation. This suggests that the initiation of the Altyn Tagh fault occurred during the deposition of unit E1+2 at 65–50 Ma (Yin et al., 2002; cf. Meyer et al., 1998).

Relationship between Upper-Crustal and Lower-Crustal Deformation

Because its topography is quite flat, the 45 km crustal thickness of the Qaidam basin may vary little under Airy isostasy. The crustal thickness of the Qaidam basin at the onset of the Indo-Asian collision was probably >~32 km, because Late Cretaceous strata are terrestrial deposits (e.g., Huang et al., 1996). With the initial (>32 km) and final (45 km) crustal thickness as the bounds, we discuss possible relationships between upper-

crustal and lower-crustal deformation during Cenozoic development of the Qaidam basin.

In the western Qaidam basin, the >48% upper-crustal shortening strain alone is sufficient to explain the observed crustal thickness (Yin et al., 2007a). This mode of deformation as shown in Figure 18A predicts an extra length of lower crust and mantle lithosphere, which may have been subducted below the neighboring thrust belts. In the eastern Qaidam basin, the observed upper-crustal shortening strain is negligible (<1%) and thus is insufficient to explain the current crustal thickness and basin elevation. The above arguments require a systematic eastward variation of crustal-thickening mechanism across the Qaidam basin: (1) dominantly upper-crustal shortening in the west (Fig. 18A), (2) mixed upper-crustal and lower-crustal thickening in the center (Fig. 18B), and (3) dominantly lower-crustal shortening in the east (Fig. 18C). The above discussion on the spatial variation of crustal shortening strain and shortening mechanisms refers only to the Qaidam basin that is defined by the present topography in the region. It is possible that the earlier extent of the Qaidam basin, such as in Paleogene time, was larger. For example, the Delingha and Sugan basins north of the Qaidam basin could once have been parts of the greater Qaidam basin.

In the absence of upper-crustal deformation, lower-crustal thickening can be achieved by channel flow (Fig. 18D) (Clark and Royden, 2000) or ductile thrusting (Fig. 18E). The first process may be tested via stratigraphic relationships. If the surface uplift rate induced by lower-crustal flow were greater than the sedimentation rate, the basin margins would migrate toward the basin center, resulting in regressional stratigraphic relationships (Fig. 19A). In contrast, if the surface uplift rate were lower than the sedimentation rate, the basin margins would migrate away from the basin center, resulting in transgressional stratigraphic relationships (Fig. 19B). As exemplified in Figure 10, the southern margin of the Qaidam basin has undergone transgression throughout the Cenozoic, which implies that the surface uplift rate induced by lower-crustal flow, if it has occurred, has been lower than the sedimentation rate. The total Cenozoic section in the southern Qaidam basin is <5 km deposited over 50 m.y., which yields an average surface uplift rate of <0.1 mm/yr.

It has been noted that the Qaidam lithosphere is unusually strong in Tibet (Braitenberg et al., 2003). If the strength of lithosphere mainly concentrates in the lower crust due to absence of fluids (i.e., Jackson et al., 2004), then Qaidam lower crust would be the least likely place for lower-crustal flow in Tibet. Thus, crustal thickening in the eastern Qaidam basin could

have been induced by thrust duplication of the lower crust (Fig. 18E). Following the inferred geometry of the Main Qaidam detachment, as shown in Figures 5, 6, 7, and 10, we envision the existence of two thrust ramps in the easternmost Qaidam; the northern thrust ramp crosses the lower crust below the Qilian Shan and the southern thrust ramp crosses the upper crust below the Eastern Kunlun Range. To explain the along-strike variation of crustal thickening, the upper-crustal ramp must lie diagonally across the Qaidam basin, as shown in Figure 14A. This ramp configuration allows progressive transition from dominantly upper-crustal shortening in the west to dominantly lower-crustal shortening in the east (Fig. 14A).

Mesozoic Deformation

Mesozoic extensional structures are widespread across the Qaidam basin. Typically, these faults cut the lower part of the Jurassic sequence but are overlain by the upper part of the sequence, suggesting that extensional faulting occurred in the Early Jurassic. This observation is inconsistent with the proposal that the Jurassic Qaidam basin was in a compressional tectonic setting (Huo and Tan, 1995; Ritts and Biffi, 2000), but consistent with the regional observation that northern and southern Tibet underwent several phases of extension in the Jurassic and Cretaceous (Huo and Tan, 1995; Huang et al., 1996; Sobel, 1999; Vincent and Allen, 1999; Kapp et al., 2000, 2003; Xia et al., 2001; Chen et al., 2003; Horton et al., 2004).

The extensional faults appear to die out along strike within a distance of 40–50 km, as we could not correlate them from one section to another like the Cenozoic structures. Because of this, the exact trends of Jurassic extensional faults are not well determined. This has made discussion on the relationship between Mesozoic and Cenozoic structures difficult. From the regional seismic sections we analyzed, we could not detect any evidence that Jurassic extensional faults were reactivated by Cenozoic thrusting (also see Yin et al., 2008; cf. Xia et al., 2001; Chen et al., 2003). Further research is needed to determine whether the lack of evidence for reactivation is due to the coarse spacing of our seismic sections, or that the trends of the older extensional faults and the younger Cenozoic thrusts are drastically different. The latter situation would make tectonic inversion difficult.

Kink Folds versus Circular Folds

Similar to our detailed structural study of the North Qaidam thrust belt (Yin et al., 2008), Cenozoic folds across the central Qaidam basin
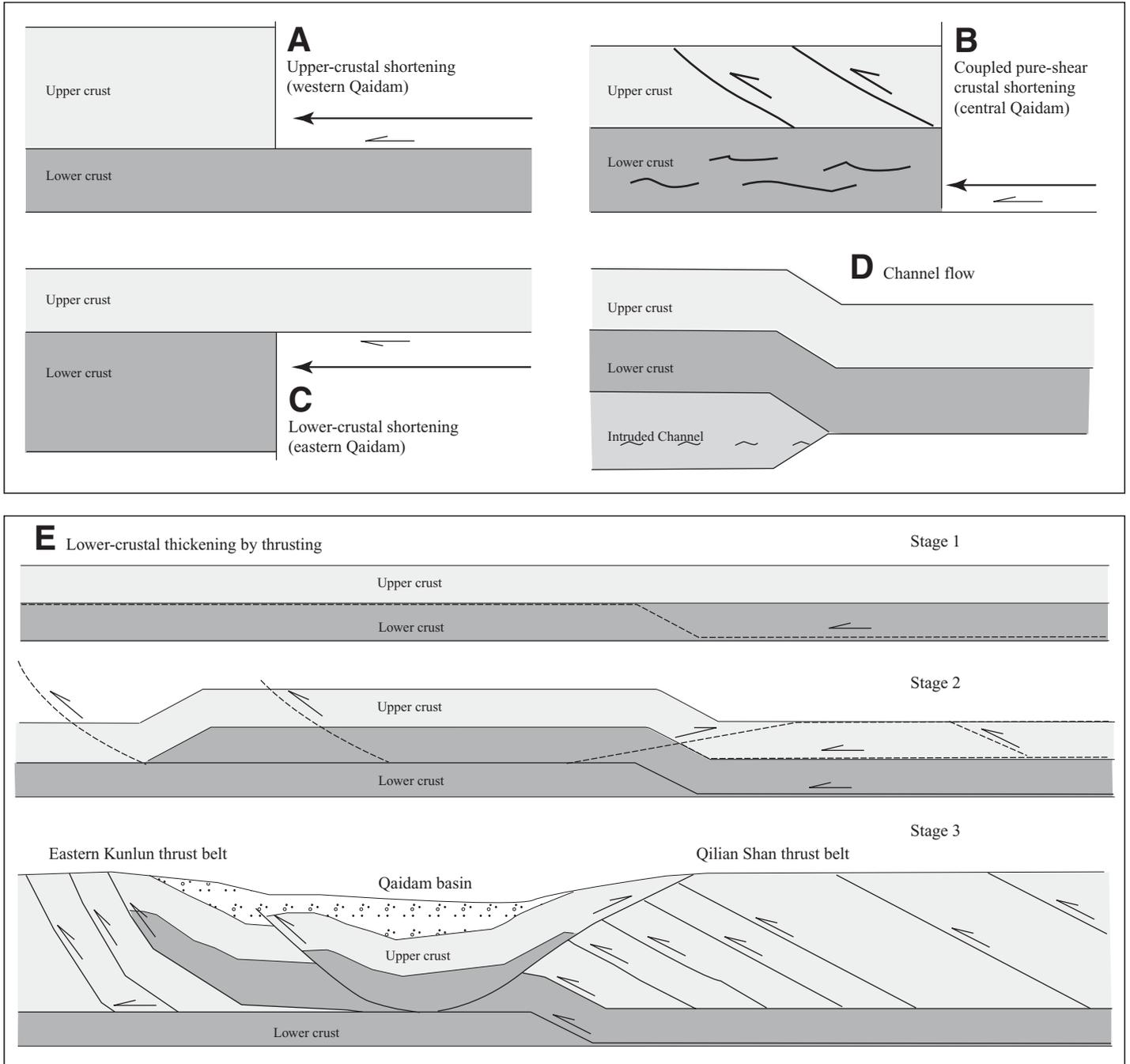
Figure 18. Relationship between upper-crustal and lower-crustal deformation across the Qaidam basin. (A) Crustal thickening is accomplished by upper-crustal shortening, and the lower crust and the mantle lithosphere are subducted below basin-bounding thrust belts. (B) Crustal thickening is accommodated by pure-shear shortening of the entire crust. (C) Crustal thickening is accommodated by pure-shear contraction in the lower crust. The extra section length for the upper crust may have been thrust over the basin-bounding thrust belts. (D) Lower crustal thickened is achieved by channel flow coming from below the basin-bounding thrust belts. (E) Crustal thickening may have been accomplished by thrust duplication of the lower crust; the brittle portion of the thrust zone may have surfaced in the Eastern Kunlun Range to the south and the listric fault geometry may cause progressive northward tilting of the basin floor, as seen in seismic lines.
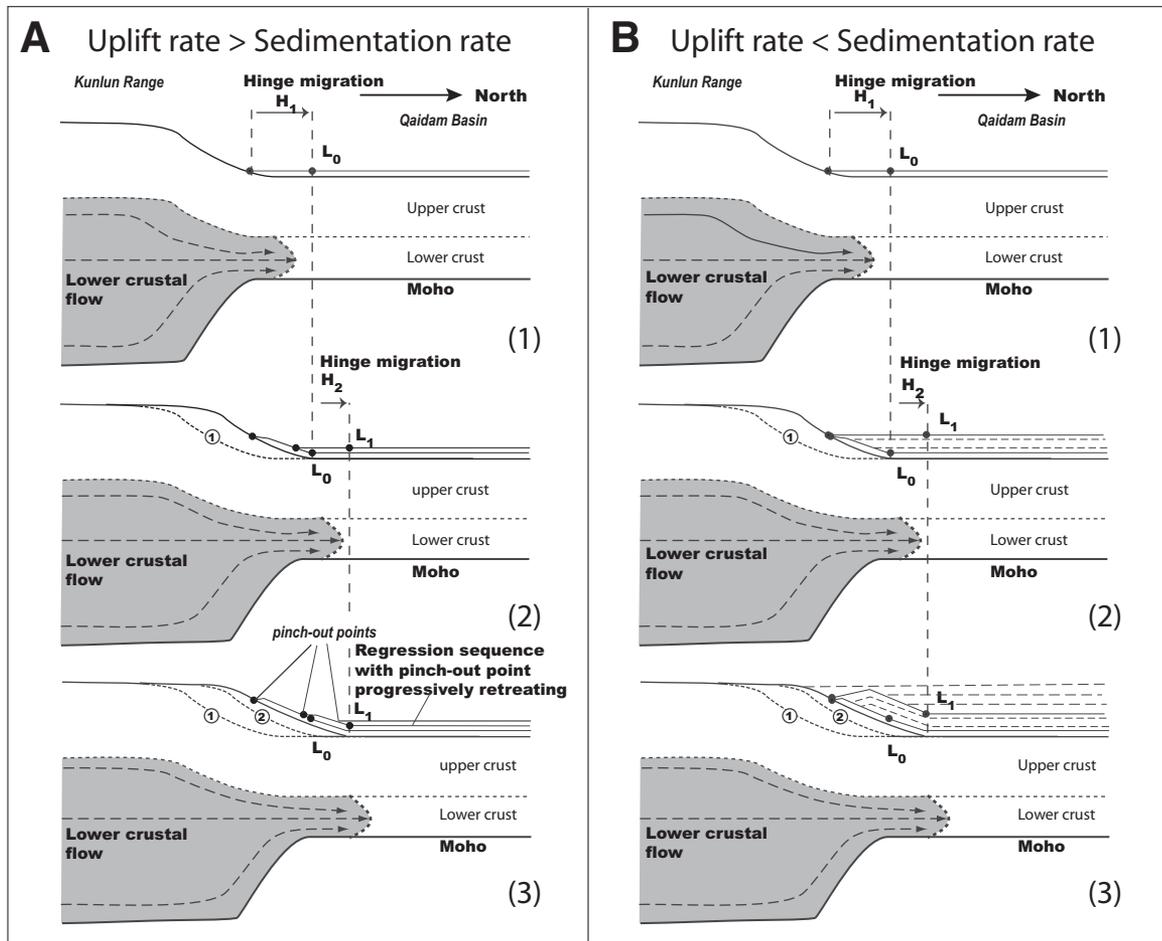
Figure 19. Possible growth-strata patterns along the northern plateau margin due to lower-crustal channel flow. (A) Sedimentation rate is lower than the uplift rate, producing a regressional sequence. (B) Sedimentation rate is higher than the uplift rate, producing a transgressional sequence.

have broader and rather circular hinge zones and lower fold amplitudes than those predicted by the kink-bend method if one extrapolates surface geology to a greater depth (Suppe, 1983). The round fold hinge-zone geometry is compatible with our direct field observations of Cenozoic folds and map patterns that show circular and broad fold-hinge zones (Yin et al., 2008). Recognition of this fold style resolves the long-noted discrepancy across the Qaidam basin that the fold limbs determined by surface mapping tend to be much steeper than those constrained by seismic and drill-hole data. That is, the broad and circular fold-hinge geometry predicts a rapid change in bedding dip downward, rather than maintaining the same dip, as anticipated by the kink-bend method.

CONCLUSIONS

The major geologic observations and inferences derived from analyses of seismic-reflection profiles and thickness distributions of Cenozoic strata across the Qaidam basin are summarized in the following.

1. The first-order structure across the basin is a major Cenozoic synclinorium, with its amplitude decreasing progressively eastward, from >16 km in the west to <4 km in the east. Associated with the amplitude decrease is an eastward decrease in the half-wavelength of the fold from ~170 km to ~50 km. Associated with the eastward decrease in fold amplitude and half-wavelength is the decrease in the north-south width of the Qaidam basin from ~400 km in the west to ~100 km in the east, suggesting that the basin formation and its topographic expression are closely related to the development of the Qaidam synclinorium. Growth-strata relationships indicate that the synclinorium axis has propagated eastward: located entirely in the western Qaidam ca. 65–50 Ma with subsequent expansion to the easternmost basin after 24 Ma.

2. Cenozoic upper-crustal shortening strain and shortening magnitude across the Qaidam basin decrease systematically eastward: >48% in the west, ~17% in the center, and <1% in the east. Cenozoic strain rates range from 1.3×10^{-17} s^{-1} to 3.2×10^{-15} s^{-1}. The eastward decrease in upper-crustal shortening strain indicates a progressive transition in crustal-thickening mechanism, from dominantly upper-crustal shortening in the west to dominantly lower-crustal shortening in the east.

3. Qaidam upper-crustal structures can be best explained by thrusting along a mid-crustal décollement, which we referred to as the Main Qaidam detachment. The detachment links a lower-crustal ramp in the northern Qaidam basin and southern Qilian Shan and an upper-crustal ramp in the southern Qaidam basin and the Eastern Kunlun Range. The depth to the décollement decreases eastward from ~28 km in the west to ~16 km in the east. The upper-crustal ramp lies diagonally across the Qaidam basin, oblique to

the general structural trend of the basin. This ramp configuration allows a systematic transition from dominantly upper-crustal shortening in the west to dominantly lower-crustal shortening in the east.

4. Although sedimentation of Paleocene–Eocene strata occurred synchronously across the entire basin, initiation of the basin-bounding structures was diachronous: the northern basin-bounding structures started coevally with the initial basin sedimentation at 65–50 Ma, while the southern basin-bounding structures started much later, at 29–24 Ma. This observation, in conjunction with the uplift of the Eastern Kunlun Range south of the basin since 30–20 Ma, suggests that the Paleogene Qaidam basin extended much farther to the south across the Eastern Kunlun Range and was possibly linked with the Paleogene Hoh Xil basin that is currently south of the Eastern Kunlun Range. The two basins formed a united Paleogene topographic depression that was >500 km wide in the north-south direction and had a size and tectonic setting similar to the present-day Tarim basin between the Tian Shan and the Tibetan plateau to the north. The development and subsequent demise of this Paleo-Qaidam basin imply a complex sequence of deformation that may have been controlled by the preexisting heterogeneity of mechanical strength in Tibetan lithosphere at the onset of the Indo-Asian collision.

5. The initiation and subsequent development of the Qaidam basin was closely related to motion on the Altyn Tagh left-slip fault. This was expressed by the Paleocene–early Eocene initiation of basin sedimentation and related deformation in the westernmost part of the basin adjacent to the strike-slip fault. Deformation and sedimentation were subsequently expanded eastward across the basin.

6. Jurassic extensional structures and associated half-grabens are widespread across the Qaidam basin. From the seismic profiles we analyzed, we could not detect any evidence that the early extensional faults were reactivated by Cenozoic thrusts.

REFERENCES CITED

Avouac, J.P., Tapponnier, P., Bai, M., You, H., and Wang, G., 1993, Active thrusting and folding along the northern Tien-Shan and late Cenozoic rotation of the Tarim relative to Zungaria and Kazakhstan: Journal of Geophysical Research, v. 98, no. B4, p. 6755–6804.

Bally, A.W., Chou, I.-M., Clayton, R., Eugster, H.P., Kidwell, S., Meckel, L.D., Ryder, R.T., Watts, A.B., and Wilson, A.A., 1986, Notes on sedimentary basins in China—Report of the American Sedimentary Basins delegation to the People's Republic of China: U.S. Geological Survey Open-File Report 86–327, 108 p.

Braitenberg, C., Wang, Y., Fang, J., and Hsu, H.T., 2003, Spatial variations of flexure parameters over the Tibet-Qinghai plateau: Earth and Planetary Science Letters, v. 205, p. 211–224, doi: 10.1016/S0012-821X(02)01042-7.

Burchfiel, B.C., Deng, Q., Molnar, P., Royden, L.H., Wang, Y., Zhang, P., and Zhang, W., 1989, Intracrustal detachment with zones of continental deformation: Geology, v. 17, p. 748–752, doi: 10.1130/0091-7613(1989)017<0448:IDWZOC>2.3.CO;2.

Burg, J.P., Davy, P., and Martinod, J., 1994, Shortening of analog models of the continental lithosphere—New hypothesis for the formation of the Tibetan plateau: Tectonics, v. 13, p. 475–483, doi: 10.1029/93TC02738.

Chen, W.P., and Molnar, P., 1983, Focal depths of intracontinental and intraplate earthquakes and their implications for the thermal and mechanical properties of the lithosphere: Journal of Geophysical Research, v. 88, p. 4183–4214.

Chen, X.H., Yin, A., Gehrels, G.E., Cowgill, E., Grove, M., Harrison, T.M., and Wang, X.F., 2003, Two phases of Mesozoic north-south extension in the eastern Altyn Tagh Range, northern Tibetan plateau: Tectonics, v. 22, p. 1053, doi: 10.1029/2001TC001336, doi: 10.1029/2001TC001336.

Chen, Y., Gilder, S., Halim, N., Cogne, J.P., and Courtillot, V., 2002, New paleomagnetic constraints on central Asian kinematics: Displacement along the Altyn Tagh fault and rotation of the Qaidam basin: Tectonics, v. 21, 1042, doi: 10.1029/2001TC901030.

Clark, M.K., and Royden, L.H., 2000, Topographic ooze: Building the eastern margin of Tibet by lower crustal flow: Geology, v. 28, p. 703–706, doi: 10.1130/0091-7613(2000)28<703:TOBTEM>2.0.CO;2.

Cloetingh, S., Burov, E., Beekman, F., Andeweg, B., Andriessen, P.A.M., Garcia-Castellanos, D., de Vicente, G., and Vegas, R., 2002, Lithospheric folding in Iberia: Tectonics, v. 21, no. 5, 1041, doi: 10.1029/2001TC901031.

Coward, M.P., Kidd, W.S.F., Pan, Y., Shackleton, R.M., and Zhang, H., 1988, The structure of the 1985 Tibet Geotraverse, Lhasa to Golmud: Royal Society of London Philosophical Transactions, ser. A, v. 327, p. 307–336, doi: 10.1098/rsta.1988.0131.

Cowgill, E., 2007, Impact of riser reconstructions on estimation of secular variation in rates of strike-slip faulting: Revisiting the Cherchen River slip rate along the Altyn Tagh fault, NW China: Earth and Planetary Science Letters, v. 254, p. 239–255, doi: 10.1016/j.epsl.2006.09.015.

Cowgill, E., Yin, A., Feng, W.X., and Qing, Z., 2000, Is the North Altyn fault part of a strike-slip duplex along the Altyn Tagh fault system?: Geology, v. 28, p. 255–258, doi: 10.1130/0091-7613(2000)28<255:ITNAFP>2.0.CO;2.

Cowgill, E., Yin, A., Harrison, T.M., and Wang, X.F., 2003, Reconstruction of the Altyn Tagh fault based on U-Pb geochronology: Role of back thrusts, mantle sutures, and heterogeneous crustal strength in forming the Tibetan Plateau: Journal of Geophysical Research, no. B7, p. 2346.

Cowgill, E., Yin, A., Arrowsmith, J.R., Feng, W.X., and Zhang, S.H., 2004a, The Akato Tagh bend along the Altyn Tagh fault, northwest Tibet 1: Smoothing by vertical-axis rotation and the effect of topographic stresses on bend-flanking faults: Geological Society of America Bulletin, v. 116, p. 1423–1442, doi: 10.1130/B25359.1.

Cowgill, E., Arrowsmith, J.R., Yin, A., Wang, X.F., and Chen, Z.L., 2004b, The Akato Tagh bend along the Altyn Tagh fault, northwest Tibet 2: Active deformation and the importance of transpression and strain hardening within the Altyn Tagh system: Geological Society of America Bulletin, v. 116, p. 1443–1464, doi: 10.1130/B25360.1.

Dang, Y., Hu, Y., Yu, H., Song, Y., and Yang, F., 2003, Petroleum geology of northern Qaidam basin: Beijing, Geological Publishing House, 187 p.

DeCelles, P.G., and Giles, K.A., 1996, Foreland basin systems: Basin Research, v. 8, p. 105–123.

Dewey, J.F., Shackelton, R.M., Chang, C., and Sun, Y., 1988, The tectonic evolution of the Tibetan Plateau: Royal Society of London Philosophical Transactions, ser. A, v. 327, p. 379–413.

Dickinson, W.R., Klute, M.A., Hayes, M.J., Janecke, S.U., Lundin, E.R., McKittrick, M.A., and Olivares, M.D., 1988, Paleogeographic and paleotectonic setting of Laramide sedimentary basins in the central Rocky Mountain region: Geological Society of America Bulletin, v. 100, p. 1023–1039, doi: 10.1130/0016-7606(1988)100<1023:PAPSOL>2.3.CO;2.

Dupont-Nivet, G., Butler, R.F., Yin, A., and Chen, X., 2002, Paleomagnetism indicates no Neogene rotation of Qaidam basin in northern Tibet during Indo-Asian collision: Geology, v. 30, p. 263–266, doi: 10.1130/0091-7613(2002)030<0263:PINNRO>2.0.CO;2.

Dupont-Nivet, G., Horton, B.K., Butler, R.F., Wang, J., Zhou, J., and Waanders, G.L., 2004, Paleogene clockwise tectonic rotation of the Xining-Lanzhou region, northeastern Tibetan Plateau: Journal of Geophysical Research, v. 109, B04401, doi: 10.1029/2003JB002620.

England, P., and Houseman, G., 1986, Finite strain calculations of continental deformation 2. Comparison with the India-Asia collision zone: Journal of Geophysical Research, v. 91, p. 3664–3676.

Gehrels, G.E., Yin, A., and Wang, X.F., 2003a, Detrital zircon geochronology of the northeastern Tibet: Geological Society of America Bulletin, v. 115, p. 881–896, doi: 10.1130/0016-7606(2003)115<0881:DGOTNT>2.0.CO;2.

Gehrels, G.E., Yin, A., and Wang, X.F., 2003b, Magmatic history of the Altyn Tagh, Nan Shan, and Qilian Shan region of western China: Journal of Geophysical Research, v. 108, 2423, doi: 10.1029/2002JB001876.

Halim, N., Chen, Y., and Cogne, J.P., 2003, A first palaeomagnetic study of Jurassic formations from the Qaidam basin, Northeastern Tibet, China—Tectonic implications: Geophysical Journal International, v. 153, p. 20–26, doi: 10.1046/j.1365-246X.2003.01860.x.

Hanson, A.D., 1998, Orogenic geochemistry and petroleum geology, tectonics and basin analysis of southern Tarim and northern Qaidam basins, northwest China [Ph.D. thesis]: Stanford, California, Stanford University, 316 p.

Harrison, T.M., Copeland, P., Kidd, W.S.F., and Yin, A., 1992, Raising Tibet: Science, v. 255, p. 1663–1670, doi: 10.1126/science.255.5052.1663.

Horton, B.K., Yin, A., Spurlin, M.S., Zhou, J.Y., and Wang, J.H., 2002, Paleocene–Eocene syncontractional sedimentation in narrow, lacustrine-dominated basins of east-central Tibet: Geological Society of America Bulletin, v. 114, p. 771–786, doi: 10.1130/0016-7606(2002)114<0771:PESSIN>2.0.CO;2.

Horton, B.K., Dupont-Nivet, G., Zhou, J., Waanders, G.L., Butler, R.F., and Wang, J., 2004, Mesozoic-Cenozoic evolution of the Xining-Minhe and Dangchang basins, northeastern Tibetan Plateau: Magnetostratigraphic and biostratigraphic results: Journal of Geophysical Research, v. 109, B04402, doi: 10.1029/2003JB002913.

Hsü, K., 1988, Relic back-arc basins: Principles of reconstruction and possible new examples from China, *in* Kleinspehn, K.L., and Paola, C., eds., New perspective in basin analysis: Berlin, Springer-Verlag, p. 345–363.

Huang, H., Huang, Q., and Ma, Y., 1996, Geology of Qaidam Basin and its petroleum prediction: Beijing, Geological Publishing House, 257 p. (in Chinese).

Huo, G.M., ed., 1990, Petroleum geology of China, *in* Oil fields in Qianghai and Xizang, v. 14: Beijing, Chinese Petroleum Industry Press, 483 p.

Huo, Y.L., and Tan, S.D., 1995, Exploration case history and petroleum geology in Jiuquan continental basin: Beijing, Chinese Petroleum Industry Press, 211 p.

Jackson, J.A., Austrheim, H., McKenzie, D., and Priestley, K., 2004, Metastability, mechanical strength, and the support of mountain belts: Geology, v. 32, p. 625–628, doi: 10.1130/G20397.1.

Jia, C., 1997, Tectonic characteristics and petroleum: Tarim Basin, China: Beijing, Chinese Petroleum Industry Press, 295 p.

Jolivet, M., Brunel, M., Seward, D., Xu, Z., Yang, J., Roger, F., Tapponnier, P., Malavieille, J., Arnaud, N., and Wu, C., 2001, Mesozoic and Cenozoic tectonics of the northern edge of the Tibetan plateau: Fission-track constraints: Tectonophysics, v. 343, p. 111–134, doi: 10.1016/S0040-1951(01)00196-2.

Jolivet, M., Brunel, M., Seward, D., Xu, Z., Yang, J., Malavieille, J., Roger, F., Leloup, A., Arnaud, N., and Wu, C., 2003, Neogene extension and volcanism in the Kunlun fault zone, northern Tibet: New constraints on the age of the Kunlun fault: Tectonics, v. 22, 1052, doi: 10.1029/2002TC001428.

Jordan, T.E., 1981, Thrust loads and foreland basin evolution, Cretaceous, western United States: American Association of Petroleum Geologists Bulletin, v. 65, p. 2506–2520.

Kang, Y.Z., ed., 1996, Petroleum geology and resource assessment in the Tarim Basin, Xinjiang, China: Beijing, Geological Publishing House, 348 p.

Kapp, P.A., Yin, A., Manning, C., Murphy, M.A., Harrison, T.M., Ding, L., Deng, X.G., and Wu, C.-M., 2000, Blueschist-bearing metamorphic core complexes in the Qiangtang block reveal deep crustal structure of northern Tibet: Geology, v. 28, p. 19–22, doi: 10.1130/0091-7613(2000)28<19:BMCCIT>2.0.CO;2.

Kapp, P., Yin, A., Manning, C.E., Harrison, T.M., Taylor, M.H., and Ding, L., 2003, Tectonic evolution of the early Mesozoic blueschist-bearing Qiangtang metamorphic belt, central Tibet: Tectonics, v. 22, no. 4, 1043, doi: 10.1029/2002TC001383.

Kidd, W.S.F., and Molnar, P., 1988, Quaternary and active faulting observed on the 1985 Academia Sinica–Royal Society Geotraverse of Tibet: Royal Society of London Philosophical Transactions, ser. A, v. 327, p. 337–363, doi: 10.1098/rsta.1988.0133.

Kong, X., Yin, A., and Harrison, T.M., 1997, Evaluating the role of preexisting weakness and topographic distributions in the Indo-Asian collision by use of a thin-shell numerical model: Geology, v. 25, p. 527–530, doi: 10.1130/0091-7613(1997)025<0527:ETROPW>2.3.CO;2.

Leeder, M.R., Smith, A.B., and Yin, J., 1988, Sedimentology, palaeoecology and palaeoenvironmental evolution of the 1985 Lhasa to Golmud Geotraverse: Royal Society of London Philosophical Transactions, ser. A, v. 327, p. 107–143, doi: 10.1098/rsta.1988.0123.

Li, S.L., Mooney, W.D., and Fan, J.C., 2006, Crustal structure of mainland China from deep seismic sounding data: Tectonophysics, v. 420, p. 239–252, doi: 10.1016/j.tecto.2006.01.026.

Li, Y.H., Wu, Q.J., An, Z.H., Tian, X.B., Zeng, R.S., Zhang, R.Q., and Li, H.G., 2006, The Poisson ratio and crustal structure across the NE Tibetan Plateau determined from receiver functions: Chinese Journal of Geophysics—Chinese Edition, v. 49, p. 1359–1368.

Liu, Y.J., Genser, J., Neubauer, F., Jin, W., Ge, X.H., Handler, R., and Takasu, A., 2005, ^{40}Ar/^{39}Ar mineral ages from basement rocks in the Eastern Kunlun Mountains, NW China, and their tectonic implications: Tectonophysics, v. 398, p. 199–224, doi: 10.1016/j.tecto.2005.02.007.

Liu, Z.F., Wang, C.S., and Yi, H.S., 2001, Evolution and mass accumulation of the Cenozoic Hoh Xil basin, northern Tibet: Journal of Sedimentary Research, v. 71, p. 971–984.

Liu, Z.F., Zhao, X.X., Wang, C.S., Liu, S., and Yi, H.S., 2003, Magnetostratigraphy of Tertiary sediments from the Hoh Xil Basin: Implications for the Cenozoic tectonic history of the Tibetan Plateau: Geophysical Journal International, v. 154, p. 233–252, doi: 10.1046/j.1365-246X.2003.01986.x.

Métivier, F., Gaudemer, Y., Tapponnier, P., and Meyer, B., 1998, Northeastward growth of the Tibet plateau deduced from balanced reconstruction of two depositional areas: The Qaidam and Hexi Corridor basins, China: Tectonics, v. 17, p. 823–842, doi: 10.1029/98TC02764.

Meyer, B., Tapponnier, P., Bourjot, L., Metivier, F., Gaudemer, Y., Peltzer, G., Shunmin, G., and Zhitai, C., 1998, Crustal thickening in Gansu-Qinghai, lithospheric mantle subduction, and oblique, strike-slip controlled growth of the Tibet plateau: Geophysical Journal International, v. 135, p. 1–47, doi: 10.1046/j.1365-246X.1998.00567.x.

Mock, C., Arnaud, N.O., and Cantagrel, J.M., 1999, An early unroofing in northeastern Tibet? Constraints from ^{40}Ar/^{39}Ar thermochronology on granitoids from the eastern Kunlun range (Qianghai, NW China): Earth and Planetary Science Letters, v. 171, p. 107–122, doi: 10.1016/S0012-821X(99)00133-8.

Molnar, P., England, P., and Martinod, J., 1993, Mantle dynamics, the uplift of the Tibetan Plateau, and the Indian monsoon: Review of Geophysics, v. 31, p. 357–396, doi: 10.1029/93RG02030.

Murphy, M.A., Yin, A., Harrison, T.M., Dürr, S.B., Chen, Z., Ryerson, F.J., Kidd, W.S.F., Wang, X., and Zhou, X., 1997, Significant crustal shortening in south-central Tibet prior to the Indo-Asian collision: Geology, v. 25, p. 719–722, doi: 10.1130/0091-7613(1997)025<0719:DTIACA>2.3.CO;2.

Neil, E.A., and Houseman, G.A., 1997, Geodynamics of the Tarim Basin and the Tian Shan in central Asia: Tectonics, v. 16, no. 4, p. 571–584, doi: 10.1029/97TC01413.

Person, M., Raffensperger, J.P., Ge, S.M., and Garven, G., 1996, Basin-scale hydrogeologic modeling: Reviews of Geophysics, v. 34, p. 61–87, doi: 10.1029/95RG03286.

Price, R.A., 1981, The Cordilleran foreland thrust and fold belt in the southern Canadian Rocky Mountains, *in* Coward, M.P., and McClay, K.R., eds., Thrust and nappe tectonics: Geological Society of London Special Publication 9, p. 427–448.

Price, R.A., 1986, The Southeastern Canadian Cordillera—Thrust faulting, tectonic wedging, and delamination of the lithosphere: Journal of Structural Geology, v. 8, p. 239–254, doi: 10.1016/0191-8141(86)90046-5.

Qinghai Bureau of Geology and Mineral Resources, 1991, Regional geology of Qinghai Province: Beijing, Geological Publishing House, 662 p.

Nansheng, Q., 2002, Tectono-thermal evolution of the Qaidam Basin, China: Evidence from Ro and apatite fission track data: Petroleum Geoscience, v. 8, p. 279–285.

Nansheng, Q., 2003, Geothermal regime in the Qaidam basin, northeast Qinghai-Tibet Plateau: Geological Magazine, v. 140, p. 707–719, doi: 10.1017/S0016756803008136.

Rieser, A.B., Neubauer, F., Liu, Y.J., and Ge, X.H., 2005, Sandstone provenance of north-western sectors of the intracontinental Cenozoic Qaidam basin, western China: Tectonic vs. climatic control: Sedimentary Geology, v. 177, p. 1–18, doi: 10.1016/j.sedgeo.2005.01.012.

Rieser, A.B., Liu, Y.J., Genser, J., Neubauer, F., Handler, R., Friedl, G., and Ge, X.H., 2006a, ^{40}Ar/^{39}Ar ages of detrital white mica constrain the Cenozoic development of the intracontinental Qaidam Basin, China: Geological Society of America Bulletin, v. 118, p. 1522–1534, doi: 10.1130/B25962.1.

Rieser, A.B., Liu, Y.J., Genser, J., Neubauer, F., Handler, R., and Ge, X.H., 2006b, Uniform Permian ^{40}Ar/^{39}Ar detrital mica ages in the eastern Qaidam Basin (NW China): Where is the source?: Terra Nova, v. 18, p. 79–87, doi: 10.1111/j.1365-3121.2005.00666.x.

Ritts, B.D., and Biffi, U., 2000, Magnitude of post-Middle Jurassic (Bajocian) displacement on the central Altyn Tagh fault system, northwest China: Geological Society of America Bulletin, v. 112, p. 61–74, doi: 10.1130/0016-7606(2000)112<0061:MOPMJB>2.3.CO;2.

Sobel, E.R., 1999, Basin analysis of the Jurassic–Lower Cretaceous southwest Tarim basin, northwest China: Geological Society of America Bulletin, v. 111, p. 709–724, doi: 10.1130/0016-7606(1999)111<0709:BAOTJL>2.3.CO;2.

Sobel, E.R., Hilley, G.E., and Strecker, M.R., 2003, Formation of internally drained contractional basins by aridity-limited bedrock incision: Journal of Geophysical Research, v. 108, 2344, doi: 10.1029/2002JB001883.

Song, S.G., Zhang, L.F., Niu, Y.L., Su, L., Jian, P., and Liu, D.Y., 2005, Geochronology of diamond-bearing zircons from garnet peridotite in the North Qaidam UHPM belt, Northern Tibetan Plateau: A record of complex histories from oceanic lithosphere subduction to continental

collision: Earth and Planetary Science Letters, v. 234, p. 99–118, doi: 10.1016/j.epsl.2005.02.036.

Song, T., and Wang, X., 1993, Structural styles and stratigraphic patterns of syndepositional faults in a contractional setting: Examples from Qaidam basin, northwestern China: American Association of Petroleum Geologists Bulletin, v. 77, p. 102–117.

Spurlin, M.S., Yin, A., Horton, B.K., Zhou, J., and Wang, J., 2005, Structural evolution of the Yushu-Nangqian region and its relationship to syncollisional igneous activity, east-central Tibet: Geological Society of America Bulletin, v. 117, p. 1293–1317, doi: 10.1130/B25572.1.

Sun, D.Q., and Sun, Q.Y., 1959, Petroleum potential of the Qaidam basin as viewed from the style and pattern of its structural geology: Journal of Geomechanics, v. 1, p. 46–57 (in Chinese).

Sun, Z., Feng, X., Li, D., Yang, F., Qu, Y., and Wang, H., 1999, Cenozoic Ostracoda and palaeoenvironments of the northeastern Tarim Basin, western China: Palaeogeography, Palaeoclimatology, Palaeoecology, v. 148, p. 37–50, doi: 10.1016/S0031-0182(98)00174-6.

Sun, Z.M., Yang, Z.Y., Pei, J.L., Ge, X.H., Wang, X.S., Yang, T.S., Li, W.M., and Yuan, S.H., 2005, Magnetostratigraphy of Paleogene sediments from northern Qaidam basin, China: Implications for tectonic uplift and block rotation in northern Tibetan plateau: Earth and Planetary Science Letters, v. 237, p. 635–646, doi: 10.1016/j.epsl.2005.07.007.

Sun, Z.M., Yang, Z.Y., Pei, J.L., Yang, T.S., and Wang, X.S., 2006, New Early Cretaceous paleomagnetic data from volcanic and red beds of the eastern Qaidam Block and its implications for tectonics of Central Asia: Earth and Planetary Science Letters, v. 243, p. 268–281, doi: 10.1016/j.epsl.2005.12.016.

Suppe, J., 1983, Geometry and kinematics of fault-bend folding: American Journal of Science, v. 283, p. 684–721.

Suppe, J., and Medwedeff, D.A., 1990, Geometry and kinematics of fault-propagation folding: Ecologae Geologicae Helvetiae, v. 83, p. 409–454.

Tapponnier, P., Peltzer, G., Le Dain, A.Y., Armijo, R., and Cobbold, P., 1982, Propagating extrusion tectonics in Asia: New insights from simple experiments with plasticine: Geology, v. 10, p. 611–616, doi: 10.1130/0091-7613(1982)10<611:PETIAN>2.0.CO;2.

Tapponnier, P., Meyer, B., Avouac, J.P., Peltzer, G., Gaudemer, Y., Shunmin, G., Hongfa, X., Kelun, Y., Zhitai, C., Shuahua, C., and Huagant, D., 1990, Active thrusting and folding in the Qilian Shan, and decoupling between upper crust and mantle in northeastern Tibet: Earth and Planetary Science Letters, v. 97, p. 382–403, doi: 10.1016/0012-821X(90)90053-Z.

Tapponnier, P., Xu, Z.Q., Roger, F., Meyer, B., Arnaud, N., Wittlinger, G., and Yang, J.S., 2001, Oblique stepwise rise and growth of the Tibet plateau: Science, v. 294, p. 1671–1677, doi: 10.1126/science.105978.

Taylor, M., Yin, A., Ryerson, F.J., Kapp, P., and Ding, L., 2003, Conjugate strike-slip faulting along the Bangong-Nujiang suture zone accommodates coeval east-west extension and north-south shortening in the interior of the Tibetan Plateau: Tectonics, v. 22, 1044, doi: 10.1029/2002TC001361.

Vincent, S.J., and Allen, M.B., 1999, Evolution of the Minle and Chaoshui Basins, China: Implications for Mesozoic strike-slip basin formation in Central Asia: Geological Society of America Bulletin, v. 111, p. 725–742, doi: 10.1130/0016-7606(1999)111<0725:EOTMAC>2.3.CO;2.

Wang, E., Xu, F.Y., Zhou, J.X., Wan, J.L., and Burchfiel, B.C., 2006, Eastward migration of the Qaidam basin and its implications for Cenozoic evolution of the Altyn Tagh fault and associated river systems: Geological Society of America Bulletin, v. 118, p. 349–365, doi: 10.1130/B25778.1.

Wang, F., Lo, C.H., Li, Q., Yeh, M.W., Wan, J.L., Zheng, D.W., and Wang, E.Q., 2004, Onset timing of significant unroofing around Qaidam basin, northern Tibet, China: Constraints from Ar-40/Ar-39 and FT thermochronology on granitoids: Journal of Asian Earth Sciences, v. 24, p. 59–69, doi: 10.1016/j.jseaes.2003.07.004.

Wang, Q., and Coward, M.P., 1990, The Chaidam Basin (NW China): Formation and hydrocarbon potential: Journal of Petroleum Geology, v. 13, p. 93–112.

Windley, B.F., Allen, M.B., Zhang, C., Zhao, Z.Y., and Wang, G.R., 1990, Paleozoic accretion and Cenozoic

redeformation of the Chinese Tien Shan Range, Central Asia: Geology, v. 18, p. 128–131, doi: 10.1130/0091-7613(1990)018<0128:PAACRO>2.3.CO;2.

Xia, W., Zhang, N., Yuan, X., Fan, L., and Zhang, B., 2001, Cenozoic Qaidam basin, China: A stronger tectonic inversed, extensional rifted basin: American Association of Petroleum Geologists Bulletin, v. 85, p. 715–736.

Yang, F., Ma, Z., Xu, T., and Ye, S., 1992, A Tertiary paleomagnetic stratigraphic profile in Qaidam basin: Acta Petrologica Sinica, v.13, p.97–101.

Yang, F., Sun, Z., Cao, C., Ma, Z., and Zhang, Y., 1997, Quaternary fossil ostracod zones and magnetostratigraphic profile in the Qaidam basin: Acta Micropalaeotologica Sinica, v. 14, p. 378–390.

Yang, P., Sun, Z., Li, D., Jing, M., Fang, F., and Liu, H., 2000, Ostracoda extinction and explosion events of the Mesozoic–Cenozoic in Qaidam basin, northwest China: Journal of Palaeogeography, v. 2, p. 69-74

Yang, J.S., Xu, Z., Zhang, J.M., Chu, C.Y., Zhang, R., and Liou, J.G., 2001, Tectonic significance of early Paleozoic high-pressure rocks in Altun-Qaidam-Qilian Mountains, northwest China, *in* Hendric, M.S., and Davis, G.A., eds., Paleozoic and Mesozoic tectonic evolution of central Asia: From continental assembly to intracontinental deformation: Geological Society of America Memoir 194, p. 151–170.

Yin, A., and Harrison, T.M., 2000, Geologic evolution of the Himalayan-Tibetan orogen: Annual Review of Earth and Planetary Sciences, v. 28, p. 211–280.

Yin, A., and Ingersoll, R.V., 1997, A model for evolution of Laramide axial basins in the southern Rocky Mountains, USA: International Geology Review, v. 39, p. 1113–1123.

Yin, A., and Kelty, T.K., 1991, Structural evolution of the Lewis thrust system, southern Glacier National Park: Implications for the regional tectonic development: Geological Society of America Bulletin, v. 103, p. 1073–1089, doi: 10.1130/0016-7606(1991)103<1073:SEOTLP>2.3.CO;2.

Yin, A., and Nie, S., 1996, A Phanerozoic palinspastic reconstruction of China and its neighboring regions, *in* Yin, A., and Harrison, T.M., eds., The tectonics of Asia: New York, Cambridge University Press, p. 442–485.

Yin, A., Harrison, T.M., Ryerson, F.J., Chen, W.J., Kidd, W.S.F., and Copeland, P., 1994, Tertiary structural evolution of the Gangdese thrust system, southeastern Tibet: Journal of Geophysical Research, v. 99, no. B9, p. 18,175–18,201, doi: 10.1029/94JB00504.

Yin, A., Nie, S., Craig, P., Harrison, T.M., Ryerson, Qian, X., and Young, G., 1998, Late Cenozoic tectonic evolution of the southern Chinese Tian Shan: Tectonics, v. 17, p. 1–27.

Yin, A., Rumelhart, P.E., Cowgill, E., Butler, R., Harrison, T.M., Ingersoll, R.V., Cooper, K., Zhang, Q., and Wang, X.-F., 2002, Tectonic history of the Altyn Tagh fault in northern Tibet inferred from Cenozoic sedimentation: Geological Society of America Bulletin, v. 114, p. 1257–1295, doi: 10.1130/0016-7606(2002)114<1257:THOTAT>2.0.CO;2.

Yin, A., McRivette, Burgess, W.P., and Chen, X., 2007a, Cenozoic tectonic evolution of Qaidam basin and its surrounding regions (Part 2): Wedge tectonics in southern Qaidam basin and the Eastern Kunlun Range, *in* Sears, J.W., Harms, T.A., and Evenchick, C.A., eds., Whence the Mountains? Inquiries into the evolution of orogenic systems: A volume in honor of Raymond Price: Geological Society of America Special Paper 433, p. 369–390, doi: 10.1130/2007.2433(18).

Yin, A., Manning, C.E., Lovera, O., Menold, C., Chen, X., and Gehrels, G.E., 2007b, Early Paleozoic tectonic and thermomechanical evolution of ultrahigh-pressure (UHP) metamorphic rocks in the northern Tibetan Plateau of NW China: International Geology Review, v. 49, p. 681-716.

Yin, A., Chen, X., McRivette, M.W., Wang, L., and Jiang, W., 2008, Cenozoic tectonic evolution of Qaidam basin and its surrounding regions (Part 1): The North Qaidam thrust system: Geological Society of America Bulletin, doi:10.1130/B26180.1.

Yuan, W.M., Dong, J.Q., Wang, S.C., and Carter, A., 2006, Apatite fission track evidence for Neogene uplift in the eastern Kunlun Mountains, northern Qinghai-Tibet Plateau: Journal of Asian Earth Sciences, v. 27, p. 847–856, doi: 10.1016/j.jseaes.2005.09.002.

Zhang, J.X., Yang, J.S., Mattinson, C.G., Xu, Z.Q., Meng, F.C., and Shi, R.D., 2005, Two contrasting eclogite cooling histories, North Qaidam HP/UHP terrane, western China: Petrological and isotopic constraints: Lithos, v. 84, p. 51–76, doi: 10.1016/j.lithos.2005.02.002.

Zhang, Y.C., 1997, Prototype of analysis of petroliferous basins in China: Nanjing, Nanjing University Press, 434 p.

Zhao, J.M., Mooney, W.D., Zhang, X.K., Li, Z.C., Jin, Z.J., and Okaya, N., 2006, Crustal structure across the Altyn Tagh Range at the northern margin of the Tibetan plateau and tectonic implications: Earth and Planetary Science Letters, v. 241, p. 804–814, doi: 10.1016/j.epsl.2005.11.003.

Zhou, J.X., Xu, F.Y., Wang, T.C., Cao, A.F., and Yin, C.M., 2006, Cenozoic deformation history of the Qaidam Basin, NW China: Results from cross-section restoration and implications for Qinghai–Tibet Plateau tectonics: Earth and Planetary Science Letters, v. 243, p. 195–210, doi: 10.1016/j.epsl.2005.11.033.

Zhu, L.P., and Helmberger, D.V., 1998, Moho offset across the northern margin of the Tibetan Plateau: Science, v. 281, p. 1170–1172, doi: 10.1126/science.281.5380.1170.